Free Energy Studies of Freezing in Slit Pores: An Order-Parameter Approach using Monte-Carlo Simulation

Ravi Radhakrishnan and Keith E. Gubbins

Department of Chemical Engineering
North Carolina State University, Raleigh, NC 27695-7905

Short Running Title:
Free Energy Studies of Freezing in Slit Pores

Corresponding Author: K.E. Gubbins

North Carolina State University
Department of Chemical Engineering
113 Riddick Labs
Raleigh, NC 27695-7905
Tel: 1-919-513-2262
Fax: 1-919-515-3465
Email: keg@ncsu.edu

Abstract

We report a molecular simulation study of freezing transitions for simple fluids in narrow slit-pores. A major stumbling block in previous studies of freezing in pores has been the lack of any method for calculating the free energy difference between the confined solid and liquid phases. Conventional thermodynamic integration methods often fail for confined systems, due to the difficulty in choosing a suitable path of integration. We use a different approach that involves calculating the Landau free energy as a function of a suitable order parameter, using the grand canonical Monte Carlo simulation method. The grand free energy for each phase can then be obtained by one-dimensional integration of the Landau free energy over the order parameter. These calculations are carried out for two types of wall-fluid interaction, a hard wall and a strongly attractive wall modeled on carbon. The grand free energy results for both cases clearly indicate a first order fluid to solid transition.

In the case of the attractive carbon wall, there are three phases. Phase A corresponds to all layers having a liquid-like structure; phase B corresponds to the contact layers (the layers adjacent to the two pore walls) being frozen and the rest of the layers being fluid-like; phase C corresponds to all the layers being frozen. Our results for the angular structure function in the individual molecular layers show strong evidence of a transition from a two-dimensional liquid phase to a hexatic phase. This is followed by a transition from the hexatic to a crystal phase.

1 Introduction

While considerable insight into liquid-gas transitions in pores (capillary condensation, wetting and layering transitions) has been gained [1], some important issues remain to be resolved for solid-fluid transitions in confined systems [2-5]. This paper addresses some of these issues through an equilibrium study of the solid-liquid transition in model slit-pores using Monte Carlo simulation.

On the experimental front, there have been several studies of melting and freezing in well characterized porous materials. Most experiments have used porous silica glasses as the confinement medium, and found a decrease in the freezing point of the confined fluid as compared to the bulk [e.g. 6,7]. Such glasses have a complex networked structure of roughly cylindrical pores, and have a narrow size distribution around a mean radius. Other experiments which reported similar trends are briefly reviewed in [3-5] and the references therein. In these studies the lowering of the freezing temperature increases as the pore width H decreases, and for larger pores (see below) is roughly proportional to $1/H$. However, an opposing trend in the freezing point shift was reported by Klein and Kumacheva [8]. The authors studied freezing of cyclohexane between parallel mica surfaces (slit shaped geometry) and observed a significant increase in the melting temperature on confinement. More recently, Castro *et. al.* [9] studied freezing of methane and other liquid alkanes on a graphite substrate by incoherent elastic neutron scattering. They found that the layer nearest to the graphite substrate melts at a temperature 10% higher than the bulk melting point of methane. A systematic experimental study to explain such contrasting behavior is very difficult, because of the lack of availability of well characterized porous materials with different pore geometries and different pore-wall interactions.

For large pores the sign of the freezing point shift ΔT_f can be explained by a classical thermodynamic treatment that produces the analog of the Kelvin equation [10]. For the

solid-fluid transition this equation is [11],

$$\frac{\Delta T_f}{T_{fb}} = -2\frac{(\gamma_{ws} - \gamma_{wl})\nu}{H\lambda_{fb}} = -\frac{\Delta\phi}{\lambda_{fb}} \tag{1}$$

where T_{fb} is the bulk freezing temperature, γ_{ws} and γ_{wl} are the corresponding wall-solid and wall-fluid surface tensions, ν is the molar volume of the liquid, λ_{fb} is the latent heat of melting in the bulk system and $\Delta\phi$ represents the difference between the total wall-solid potential energy and the wall-solid potential energy that would exist if the wall were made up of the adsorbed solid itself. This type of classical thermodynamic argument breaks down for small pores, as the concept of surface tension is not well defined in the limit of small and highly inhomogeneous systems.

Several molecular simulation studies [3-5] have been carried out recently in an attempt to explain the differences in the freezing point behavior. The obvious advantage in using this approach is that one can control the model parameters precisely, and so isolate the effects of pore geometry and pore wall strength on the observed phenomena. Miyahara and Gubbins [3] studied freezing of Lennard-Jones methane in slit-shaped pores with different pore-wall interactions. They concluded that the shift in freezing temperature from the bulk value (ΔT_f), was positive if the fluid-wall interaction is more strongly attractive than the fluid-fluid interaction and negative if the fluid-wall interaction was less attractive than the fluid-fluid interaction (figure 1). Maddox and Gubbins [4] studied freezing and melting of simple fluids in pores of cylindrical geometry, and reached similar conclusions. However, they found important differences because of the increased confinement in a cylindrical geometry. In particular, the additional confinement led to downward shifts in the freezing temperatures when compared to confinement in a slit geometry. These findings provide a qualitative understanding of the freezing/melting behavior observed in the experiments. However, a limitation of both of these the simulation studies was that the precise location of the phase transition was not found. The freezing and melting displayed large hysteresis loops, and thus the location of the equi-

librium freezing/melting point could be estimated only to the accuracy of the width of the hysteresis loops. The nature of the transition was also not clear, and the continuous nature of the freezing curves suggested that the phase transition could be continuous.

In an attempt to address this problem, Dominguez *et al.* [5] used thermodynamic integration [12] to calculate the free energy of the solid and fluid phases in the pore. This method involves a numerical integration of the Gibbs free energy starting from a known reference phase (the Einstein crystal for the solid phase and the ideal gas for the liquid phase) to the state point of interest. It relies on finding a suitable path of integration which is thermodynamically reversible, i.e., the path does not intersect any phase boundary characterized by a first order transition. Thus, the free energy study in Ref. [5] was limited to confined systems with repulsive or weakly attractive wall-fluid potentials. For the more ubiquitous case of a wall-fluid potential that is moderately or strongly attractive, this method breaks down. This is because the adsorbed molecules adjacent to the pore-wall (the contact layer) freeze before the adsorbed molecules in the interior of the pore, (see figure 3 (b) in section 3.2). This makes it impossible to find a reversible path from the ideal gas phase to the fluid phase, since any such path runs into a first order transition corresponding to the freezing of the contact layer [13].

In this paper we use an approach based on the Landau theory of phase transitions to calculate the free energy difference between solid and fluid phases in confined systems. The method is similar to that used by Lynden-Bell *et. al.* [14] to study melting and freezing of bulk platinum, and we show that it works for all kinds of fluid-wall potentials, provided that a suitable order parameter is used. We study the freezing of Lennard-Jones methane in slit-shaped pores. We consider two kinds of pore-wall interactions, a hard wall that corresponds to a purely repulsive fluid-wall interaction, and a graphite wall for which the fluid-wall interaction is strongly attractive. The rest of the paper is organized as follows: in section 2, we discuss the various potential models and simulation methods and

also describe the formulation of the free energy method used. Our results are described in section 3. Sections 3.1 & 3.2 show the free energy calculation. We investigate the quasi-two-dimensional nature of the fluid phase in the case of a graphite pore in section 3.3. In section 3.4, the mechanism of hysteresis occurring in the freezing/melting process is discussed from an equilibrium perspective, and finally in section 4, we point out some areas for future work along with our conclusions.

2 Simulation methodology

2.1 Potential models

The interaction between the adsorbed fluid molecules is modeled using the Lennard-Jones (12,6) potential with size and energy parameters chosen to describe methane. Two types of pores, (1) a purely repulsive and smooth hard wall pore, and (2) a graphite pore, are chosen to study the effect of a purely repulsive and a highly attractive fluid-wall potential on the freezing point of methane.

Our model of the repulsive pore is characterized by a pore width H, which is defined to be the distance between the planes through the nuclei of the atoms in the first atomic layer of each of the opposing walls. The repulsive wall can be thought of as being composed of a continuum of hard sphere atoms. The hard sphere diameter in our model is chosen to be the same as the Lennard-Jones size parameter, $\sigma_{fw} = 0.361$ nm, that characterizes the methane-graphite interaction, which is discussed below.

To model the graphite pore, we use the integrated 10-4-3 Steele potential [15,16] given by,

$$\phi_{fw}(z) = 2\pi\rho_w\epsilon_{fw}\sigma_{fw}^2\Delta\left[\frac{2}{5}\left(\frac{\sigma_{fw}}{z}\right)^{10} - \left(\frac{\sigma_{fw}}{z}\right)^{4} - \left(\frac{\sigma_{fw}^4}{3\Delta(z+0.61\Delta)^3}\right)\right] \qquad (2)$$

The potential parameters for methane and for the graphite wall were taken from Steele [15,16],

$$\begin{aligned}
&\sigma_{ff} = 0.381 \text{ nm}, && \epsilon_{ff}/k_B = 148.1 \text{ K} \\
&\sigma_{ww} = 0.340 \text{ nm}, && \epsilon_{ww}/k_B = 28.0 \text{ K} \\
&\rho_w = 114 \text{ nm}^{-3}, && \Delta = 0.335 \text{ nm} \\
&\sigma_{fw} = (\sigma_{ff} + \sigma_{ww})/2, && \epsilon_{fw} = (\epsilon_{ff}\epsilon_{ww})^{1/2}
\end{aligned}$$

Here, the σ's and ϵ's are the size and energy parameters in the Lennard-Jonnes (LJ) potential, the subscripts f and w denote fluid and wall respectively, z is the coordinate perpendicular to the pore walls and k_B is the Boltzmann's constant. For a given pore width H, the total potential energy from both walls is given by,

$$\phi_{pore}(z) = \phi_{fw}(z) + \phi_{fw}(H - z) \tag{3}$$

We expect the approximation of a structureless graphite wall to be a good one here, since the diameter of the LJ molecule (0.381 nm) is much larger than the C–C bond length in graphite (0.14 nm), so that methane molecules only feel a mild corrugation in the fluid-wall potential in passing along the surface. This has been confirmed by simulations of monolayers of methane on structured, planar carbon walls [17], where wall structure had only a minor effect for temperatures down to 60 K. This argument was further tested in Ref. [3], where it was found that the structure of methane was practically identical when confined between smooth and structured graphite pore walls, for both the fluid as well as the solid phase.

The simulation runs were all performed in the grand canonical ensemble as described in Ref. [18], fixing the chemical potential μ, the volume V of the pore and the temperature T. The pore width in the simulation was typically around $7.5\sigma_{ff}$, and the cuboidal simulation cell was $10\sigma_{ff}$ by $10\sigma_{ff}$ in the plane parallel to the pore walls, consistent with a cutoff of $5\sigma_{ff}$ for the fluid-fluid interaction. The system typically had up to 700 particles, and periodic boundary conditions were employed in the plane parallel to the

pore walls. The simulation was setup such that insertion, deletion and displacement moves were attempted with equal probability, and the displacement step was adjusted to have a 50% probability of acceptance. Thermodynamic properties were averaged over 40-100 million individual Monte Carlo steps. The length of the simulation was adjusted such that a minimum of ten times the average number of particles in the system would be inserted and deleted during a single simulation run.

2.2 Free energy formulation

2.2.1 Landau free energy

In the Landau theory of phase transitions [19,20], the model system is characterized by an order parameter Φ, which is generically a density variable that takes on distinct values in different phases of the system. The behavior of Φ as a function of the state variables in the thermodynamic limit determines the nature of the phase transition. In particular, the probability $P[\Phi]$ of observing the system having an order parameter value between Φ and $\Phi + \delta\Phi$ assumes a bi-modal distribution when there is two-phase coexistence. As the state conditions are varied, the relative behavior of the two peaks with respect to each other provides information on which phase is more stable in the thermodynamic sense. The probability distribution function $P[\Phi]$ is calculated during a simulation run by collecting statistics of the number of occurrences of a particular value of Φ in the form of a histogram. For the general case of a spatially varying order parameter $\Phi(\vec{x})$, the probability $P[\tilde{\Phi}]$ is defined as,

$$P[\tilde{\Phi}] = \frac{1}{\Xi} \sum_{N=1}^{\infty} \frac{\exp(\beta\mu N)}{N!\lambda^{3N}} \int D_N[\Phi(\vec{x})]\, \delta(\tilde{\Phi} - \Phi)\, \exp(-\beta H_N) \tag{4}$$

Ξ is the partition function in the grand canonical ensemble, N the number of molecules in the system, $\beta = 1/k_B T$, λ is the de Broglie wavelength and H_N is the Hamiltonian of

the system. The path integral notation $D_N[\Phi(\tilde{\vec{x}})]$ should be interpreted as [20],

$$\int D_N[\Phi(\vec{x})] \equiv \lim_{v_o \to 0} \Pi_\alpha \int d\Phi_\alpha = \int_{\vec{r}^N} d\vec{r}^N \tag{5}$$

Equation (5) defines the path integral in terms of a trace over a discrete number of sites α, and v_o represents the volume per site. The Landau free energy $\Lambda[\tilde{\Phi}]$ is then defined as,

$$\exp(-\beta\Lambda[\tilde{\Phi}]) = \sum_{N=1}^{\infty} \frac{\exp(\beta\mu N)}{N!\lambda^{3N}} \int D_N[\Phi(\vec{x})]\, \delta(\tilde{\Phi} - \Phi)\, \exp(-\beta H_N) \tag{6}$$

and can be interpreted as the free energy corresponding to a restricted partition function in order parameter space. From this definition it follows that,

$$\Lambda[\Phi] = -k_B T \ln(P[\Phi]) + Constant \tag{7}$$

The grand free energy $\Omega = -k_B T \ln(\Xi)$, is then related to the Landau free energy by,

$$\exp(-\beta\Omega) = \int d\Phi \exp(-\beta\Lambda[\Phi]) \tag{8}$$

We use equation (7) to calculate the Landau free energy from the probability distribution function and then use equation (8) to calculate the grand free energy. This approach was first used to study solid-fluid transitions in the bulk by van Duijneveldt *et al.* [14,21].

2.2.2 Umbrella sampling

To overcome the difficulty of collecting reliable statistics on the probability distribution function we used umbrella sampling [22]. To calculate $P[\Phi]$, the order parameter space is divided into ten windows. As a first estimate, an approximate probability distribution $P_1[\Phi]$ was calculated separately in each of the windows, by collecting statistics in the form of a histogram in Φ without the use of any weighting function in the umbrella sampling. A sucessive set of simulations were then performed in each of the windows by using a weighting function $w\{\Phi\} = (P_1[\Phi])^{-1}$, in addition to the usual acceptance criteria for the probabilities in the GCMC simulation [14].

This process can be interpreted as performing the simulation in a new ensemble, $\Psi(T, V, \mu, h)$, which is related to the Λ-ensemble $\Lambda(T, V, \mu, \Phi)$, by the Legendre transformation

$$\Psi(T, V, \mu, h) \;=\; \Lambda(T, V, \mu, \Phi) \;-\; h\Phi \tag{9}$$

where the term $-h\Phi \equiv w\{\Phi\}$ is the weighting function in the umbrella sampling. Thus, using the weighting function in the acceptance criteria of the GCMC simulation is like applying an external field h that is conjugate to the order parameter Φ. At the coexistence condition, it is this field that forces the system to move from one stable minimum to the other. For this method to work successfully, it is important to choose an appropriate order parameter Φ which responds to changes in h; Φ should act as a conjugate variable to h [14]. It is equally important to ensure that the choice of $w\{\Phi\}$ causes the regions of Φ that are thermodynamically unstable in the Λ-ensemble, to be thermodynamically stable in the Ψ-ensemble. These two conditions ensure ergodicity and the collection of reliable statistics, respectively. The Landau free energy $\Lambda[\Phi]$ is recovered from the Ψ-ensemble using equation (9).

2.3 Order parameter

In order to study solid-liquid phase transitions, the order parameter should be sensitive to the degree of crystalline order in the system. We followed the previous work on bulk fluids [14,21] in using an order parameter that measures the orientational order (a measure of the rotational symmetry of the crystal). Our calculations of the adsorption vs. temperature, and of the radial distribution function, showed that the behavior of methane was qualitatively different in the hard wall pore and in the graphite pore. We used these results as a basis to choose a suitable order parameter.

2.3.1 Hard wall pore

The adsorption curve and the three-dimensional pair correlation functions were calculated for methane confined in a hard wall pore of width $7.5\sigma_{ff}$ using standard GCMC simulations. The chemical potential was maintained at a value corresponding to a pressure of 100 atm.; a LJ equation of state from the literature [23] was used to relate the chemical potential to the pressure. This high pressure is necessary to study hard wall systems because the methane would evaporate inside such pores under normal pressures [3]. These results indicated that the structure of the fluid and solid phases were similar to the bulk three-dimensional structure, but the transition itself was occurring at a much lower temperature than for bulk methane; the freezing of Lennard-Jones methane in the bulk occurs at $T = 101K$ [24,25]. Thus, three dimensional bond orientational order parameters introduced by Steinhardt *et al.* [26] (see also Refs. [14,21]) are employed. These order parameters are defined as follows: each nearest neighbor bond has a particular orientation in space with respect to a reference axis, which can be described by the spherical coordinates (θ, ϕ). Nearest neighbors were identified as those particles that were less than a cutoff distance r_{nn} away from a given particle. We used a cutoff distance $r_{nn} = 1.3\ \sigma_{ff}$, corresponding to the first minimum of $g(r)$ in a fcc crystal at bulk coexistence [27]. One can then define the global order parameter $\overline{Q}_{lm}$ [28],

$$\overline{Q}_{lm} \ = \ \frac{1}{N_b} \sum_{i=1}^{N_b} Y_{lm}(\theta_i, \phi_i) \tag{10}$$

where the index i runs over the total number of nearest neighbor bonds N_b and the Y_{lm}'s denote the spherical harmonics. In order that the order parameter does not depend on the overall orientation of the crystal in the simulation cell, rotationally isotropic combinations of the $\overline{Q}_{lm}$'s are defined as [28],

$$Q_l \ \equiv \ \left(\frac{4\pi}{2l+1} \sum_{m=-l}^{+l} \left| \overline{Q}_{lm} \right|^2 \right)^{1/2} \tag{11}$$

and,

$$W_l = \frac{1}{\left(\sum_m \left|\overline{Q}_{lm}\right|^2\right)^{3/2}} \sum_{m_1,m_2} \begin{pmatrix} l & l & l \\ m_1 & m_2 & -m_1-m_2 \end{pmatrix} \overline{Q}_{lm_1}\overline{Q}_{lm_2}\overline{Q}_{l(-m_1-m_2)} \qquad (12)$$

The matrix in equation (12) is a representation of the Wigner $3J$ symbols defined in Ref. [29]. The value of the order parameters for some common crystal types are given in Table 1. From the positions of the first five peaks in the pair correlation function of the solid phase (at $r/\sigma_{ff} = 1, \sqrt{2}, \sqrt{3}, 2, \& \sqrt{5}$), it was evident that the crystal structure could either be a simple cubic lattice or a face centered cubic lattice. The calculation of the order parameters showed that,

$$\begin{aligned} Q_6 &= 0.505, \qquad & Q_4 &= 0.159 \\ W_6 &= -0.0128, & W_4 &= -0.151, \end{aligned}$$

confirming that the crystal structure was a face centered cubic lattice. We therefore followed Lynden-Bell *et. al.* [14], and used the combination $\Phi = Q_6 - 3W_4$ as the order parameter for the Landau free energy calculation. The quantity Q_6 alone is a good order parameter in terms of being able to distinguish the fluid phase from a solid phase, but it is the quantity Φ that responds to the external field in the umbrella sampling method.

2.3.2 Graphite pore

For methane adsorbed in the graphite pore ($H = 7.5\sigma_{ff}$), the adsorption curve was calculated along a path such that, for each temperature, the value of the chemical potential corresponded to the pressure at which there is two-phase (gas-liquid for temperatures above the triple point and gas-solid line below the triple point) coexistence in the bulk fluid [24,25]. This path was chosen so that our calculations could be verified in a real experiment, without having to depend on an accurate LJ equation of state [3]. In figure 2 the density profile along the z direction (the direction perpendicular to the pore walls)

is shown. In contrast to the behavior for hard wall confinement, distinct layering occurs for the whole range of temperatures for which freezing and melting occur. The order in each of the individual layers is studied by calculating the in-plane, two-dimensional pair correlation functions within each layer (see figure 3). The plots in figure 3 indicate that the contact layers (the two layers adjacent to the pore walls) freeze at a temperature higher than the rest of the layers. The large value (about 4.5) of the first peak in $g(r)$ for the contact layer, a first minimum of zero, and the split second and third peaks, all show evidence of a solid phase in this layer. These results are consistent with those obtained by Miyahara and Gubbins [3] and by Dominguez *et al.* [5] for similar systems. Miyahara and Gubbins also verified the Hansen-Verlet criterion [30] for freezing by calculating the structure factor. This criterion is based on the value of the first peak in the structure factor, $S(k_o)$, and states that in the solid phase $S(k_o) \geq 2.7$ in three dimensions and $S(k_o) \geq 4.4$ in two dimensions. In order to capture the layer-by-layer freezing behavior, we chose to use a two-dimensional order parameter previously introduced by Mermin [31,32],

$$\Phi_j = \left| \frac{1}{N_b} \sum_{i=1}^{N_b} \exp(i6\theta_i) \right| = \left| \langle \exp(i6\theta_i) \rangle_j \right| \tag{13}$$

Φ_j measures the hexagonal crystalline bond order within each layer j. The overall order parameter Φ is an average of the hexagonal order in all the layers.

$$\Phi = \left(\sum_{j=1}^{N_{layers}} \Phi_j \right) / N_{layers} \tag{14}$$

For molecules with isotropic interaction potential the only two-dimensional closed packed structure is the hexagonal crystal. The quantity Φ is invariant under rotation about the z axis. We expect $\Phi = 0$ when all the layers have the structure of a two-dimensional liquid (figure 3 (a)), $\Phi = 1$ in the solid phase (figure 3 (c)) and $0 < \Phi < 1$ for the phase in figure 3 (b).

3 Results

3.1 Hard wall pore

The variation of adsorption with temperature for LJ methane confined in the hard wall pore of width $H = 7.5\sigma_{ff}$ indicated that freezing occurred at a temperature $T \simeq 40K$, and melting occurred at a temperature $T \simeq 80K$. Thus, a pronounced hysteresis loop occurs, spanning about $40K$. The Landau free energy, $\Lambda[\Phi]$, is shown in figure 4 for two different temperatures, $T = 60K$ and $T = 45K$; it has a double well structure, with the broad minimum centered around $\Phi = 0$ corresponding to the liquid phase and the second minimum centered around $\Phi = 0.95$ corresponding to the face centered cubic solid phase (ideally, $\Phi_{fcc} = 1.052$). The high temperature curve shows the liquid phase to be more stable, while the low temperature curve shows the crystal phase to be the most stable. The Landau free energy curves in figure 4 are determined up to an arbitrary constant. The grand free energy for each phase is calculated from the Landau free energy using equation (8), by evaluating the integral numerically over the order parameter range characterizing the particular phase. This calculation determines the relative free energy difference between the liquid and solid phases at a particular temperature. To relate the grand free energy of a particular phase at two different temperatures, we numerically integrate

$$\left[\frac{\partial\Omega}{\partial\mu}\right]_{T,V} = -N \tag{15}$$

to obtain Ω as a function of μ at constant temperature, and

$$\left[\frac{\partial(\Omega/T)}{\partial(1/T)}\right]_{\mu,V,A} = U - N\mu \tag{16}$$

to obtain Ω as a function of T at constant chemical potential. In equation (16), U is the total internal energy of the system. A suitable reversible path of integration can always be chosen either along the melting or the freezing branch of the adsorption curve. The grand free energy for the liquid and the crystal phase as a function of temperature is

shown in figure 5. The crossover of the liquid and solid branches at different slopes clearly establishes the transition as first order, and also determines the transition point at $T = 48K$, which should be compared to the bulk transition of $T = 101K$ for LJ methane. The free energy surface formed by the locus of points representing the stable thermodynamic phase is convex upwards, as required by the thermodynamic stability criterion (e.g. [33]). The free energy calculation in figure 5 is consistent with that obtained by Dominguez *et al.* [5] for the hard wall case using the method of Frenkel and Ladd [12], and is presented here just to establish the validity of the Landau free energy method, before applying it to the more interesting case of confinement in an attractive fluid-wall potential.

We note that the true equilibrium freezing temperature of 48 K is lower than that inferred for a system of $H = 7.5\ \sigma_{ff}$ from the work of Miyahara and Gubbins [3]; in that work a sharp rise in the density of the confined material occurred at about 70 K, on cooling. However, we note that the *effective* pore width for the present system is less than that used in [3], since the hard sphere diameter of the wall molecules was chosen to be σ_{fw} of methane-carbon interaction in our study, whereas in [3] it was $0.84\sigma_{fw}$. Thus the effective pore width, $W = H - \sigma_{fw}$ in the present work, is less than that of Ref. [3] by $0.32\ \sigma_{fw}$. This decrease in W is believed to be responsible for the difference in freezing temperatures.

3.2 Graphite pore

The Landau free energy as a function of the average hexagonal bond order Φ as defined in equations (13,14) is shown in figure 6 for four different temperatures for methane confined in the graphite pore of pore width $7.5\sigma_{ff}$. Unlike the hard wall confinement case (or the bulk behavior), this system is characterized by three phases A, B and C corresponding to the three minima in figure 6. The structure of the three phases has already been shown in figure 3. In phase A, all the layers have an isotropic liquid-like structure; phase B

is characterized by frozen contact layers, with the rest of the layers having an isotropic structure; and in Phase C, all the layers are frozen. The relative stability of the three phases as a function of temperature can be pictured qualitatively from the positions of the minima in the Landau free energy curves. The freezing point of the contact layers and that of the inner layers were determined exactly by calculating the grand free energy, which depends on the positions as well as the width of each minimum. This calculation is depicted in figure 7 for the three phases A, B and C. The plot indicates two first order transitions, one at $T = 124K$ corresponding to the freezing of the contact layers and the other at $T = 114K$ corresponding to the freezing point of the inner layers (see Table 2). For the adsorption vs. T curve (see figure 12), it is clear that the jump in the number of molecules corresponds to the freezing of the inner layers, as the temperature $T = 114K$ falls in between the hysteresis loops.

The equilibrium freezing temperature found here, 114 K, is somewhat lower than the freezing temperature of 118 K found in Ref. [3] by observing the rise in adsorbate density as the system is cooled. Although the model and pore width used in the two cases are identical, we note that in [3] the ideal gas equation of state was used to relate the chemical potential and pressure of the coexisting bulk gas. In the present case, the virial equation of state was used instead; this modification yielded chemical potentials that were up to 10 % different from the ideal gas values. Although the difference is small, we note that, because of the small difference in the slope of the grand free energy vs. T curves shown in figure 7 for the three phases, such a change can affect the calculated melting/freezing temperature significantly. Thus, we believe the freezing temperature determined here is more accurate than that inferred in Ref. [3].

As far as we are aware, this is the first calculation of the free energies and the thermodynamic freezing points in confined systems with a generic fluid-wall potential. Comparing the grand free energy results for the hard wall pore and the graphite pore (figure 5 and

figure 7), we conclude that the freezing transition in the graphite pore case is a weak first order transition, as compared to the strong transition in the hard pore case. This is indicated by the magnitude of the discontinuity in the slope of the free energy curve at the transition point, which is a measure of the first order jump in the heat capacity. The nature of the fluid phases A and B, and the reason for the freezing transition being weakly first order, are discussed in section 3.3.

3.3 Quasi-two-dimensional behavior

Care is needed in interpreting the isotropic two-dimensional pair correlation functions corresponding to all the layers in figure 3 (a) and the inner layers in figure 3 (b). Although the plots of the isotropic pair correlation functions are reminiscent of those of a two-dimensional liquid, a closer look at the third peaks of the $g(r)$ functions in figure 3 (a) reveals that the contact and the second layers have extended positional correlations compared to the inner layers. Secondly, the value taken by the order parameter Φ in phase A is about 0.24 (figure 6) as compared to the expected value close to zero if all the layers were liquid. Similarly the value of Φ in phase B is 0.5, which is much larger than the expected value of 2/7 if the contact layers are frozen ($\Phi_1 = \Phi_7 = 1$), and the inner layers are assumed to to have the structure of a liquid ($\Phi_i = 0$, $i = 2\,\text{to}\,6$). Such intermediate values for Φ suggest the occurrence of an intermediate phase with bond-orientational order.

Two-dimensional systems have a special significance for phase transitions in which continuous symmetry is broken (such as freezing transitions). The Mermin-Wagner theorem [34] states that long range order (LRO) cannot exist in such systems. The two-dimensional XY model of spins falls into this category, and Kosterlitz and Thouless [35] showed that there can still be a continuous phase transition from the disordered phase (where the two point correlation function decays exponentially) to a quasi-long range

ordered (QLRO) phase (where the two point correlation function decays algebraically). The QLRO phase is characterized by bound pairs of vortices (topological defects) with opposite sense. The Kosterlitz-Thouless (KT) transition describes the unbinding of a dilute gas of vortex-pairs through a renormalization-group treatment. The existence of the isolated vortex spin states causes the system to be disordered. The KT transition is accompanied by a non-universal peak in the specific heat above the transition temperature, associated with the entropy liberated by the unbinding of the vortex pairs.

Halperin and Nelson proposed a mechanism for melting of a crystal in two dimensions [32] which involved two KT-like transitions. The first is a transition between the crystal phase (having positional QLRO and orientational LRO) and a hexatic phase (having positional disorder and orientational QLRO); the second transition is between the hexatic phase and the liquid phase (having positional and orientational disorder). The crystal to hexatic transition occurs through the unbinding of dislocation pairs, and the hexatic to liquid transition involves the unbinding of disclination pairs. In two dimensions, the only close packed structure for circular disks with isotropic interaction is the hexagonal lattice. A disclination is then characterized by a local configuration in which a molecule has five or seven nearest neighbors instead of the usual six. A disclination pair is a bound state of a five and a seven nearest neighbor configuration. A dislocation can be viewed as a pair of disclination pairs. A complete review of the mechanism of two dimensional melting is given in Ref. [36].

The hexatic phase was first observed experimentally in liquid crystals. In between the smectic-A phase and the crystal-B phase, a hex-B phase exists that possesses long range orientational order. This was detected in an electron diffraction experiment on liquid crystalline thin films [37], in which the intensity pattern displayed a sixfold symmetry of diffuse spots indicating positional disorder but long range orientational order. The intensity pattern for a smectic-A phase is a uniform ring and that of the crystal-B phase

has six Bragg peaks corresponding to a two-dimensional hexagonal lattice. These layered liquid-crystalline systems are quasi-two-dimensional because of the additional interaction of molecules between layers. It is believed that this inter-layer interaction causes the crystal phase to have true long range positional and orientational order, and the hexatic phase to have true long range orientational order (and positional QLRO), and therefore the hexatic to crystal transition is first order, unlike the strictly two-dimensional case [38]. The nature of layer by layer freezing in a free standing film of smectic-A phase with four molecular layers was investigated by Chao *et al.* [39]. The transitions were probed using heat capacity and shear modulus measurements as well as electron diffraction patterns. Specific heat peaks were observed for the liquid-hexatic transitions but not for the hexatic-crystal transitions because most of the entropy change occurs in the former transition. However the shear modulus increased from zero continuously as the hexatic-crystal transition occurred. These measurements, together with the diffraction patterns, revealed that both the liquid-hexatic and the hexatic-crystal transitions in the two edge layers occurred at higher temperatures compared to those in the two inner layers.

The spontaneous ordering of the adsorbed molecules in the graphite pore into distinct two-dimensional layers (figure 2) is analogous to the structure of a smectic-A phase in liquid crystals. Thus the nature of the freezing transitions in the individual layers of methane can be studied along the same lines as freezing in the free standing liquid crystalline films. In figure 8 we show the heat capacity of the whole system and the order parameter in the individual layers as a function of temperature as the system is cooled. The i^{th} layer is a liquid for the range of temperatures for which $\Phi_i = 0$ and is a solid when $\Phi_i \simeq 0.85$. The first peak in the specific heat that occurs close to $T = 127K$ indicates a liquid to hexatic phase transition in the contact and second layers, as seen from the continuous increase in the order parameter value in these layers. Similarly, the second peak in the specific heat at $T = 114K$ indicates a liquid to hexatic transition in the third and the middle layers. The hexatic to crystal transition is expected to

produce a discontinuity in the specific heat, which is probably too small to be seen in figure 8 for the same reason as in the case of the liquid crystalline film [39]. The structure factor $I(k_x, k_y)$ (equivalent to the intensity pattern in the electron diffraction experiment) was also calculated to support the interpretation of the above trends. Figures 9 & 10 show the in plane structure factor for the contact and the third layers at four different temperatures. The intensity patterns in the form of a uniform ring suggests a liquid structure at $T = 160K$. The structure factor at $T = 128K$ (figure 9 (b)) shows a six fold symmetry in the intensity pattern in the contact layers supporting the onset of the hexatic transition in the contact layer, as indicated by the specific heat peak at that temperature. The third and the middle layers however, have the intensity pattern of a liquid (figure 10 (b)). The structure at $T = 111K$ (figures 9 & 10 (c)) is consistent with the existence of a hexatic phase in the second, third and the middle layers and a solid phase in the contact layers (as indicated by the highly peaked structure of the intensity pattern). Finally, the structure factor at $T = 101K$ (figures 9 & 10 (d)) shows all the layers having the structure of a hexagonal crystal. In the structure factor plots, the difference between the hexatic and the crystal phase patterns can be seen from the height and the width of the peaks in the intensity pattern. The reason for the crystal phase pattern having peaks of finite width is the finite size of the simulation cell. The structure factor patterns are consistent with the specific heat behavior in figure 8. In addition, the defect structures in these phases were analyzed using snapshots of molecular configurations. The molecular positions in the crystal phase correspond to a defect free hexagonal crystal (figure 11 (a)). The hexatic phase configurations (figure 11 (b)) show bound disclination pairs; there is also sufficient orientational order in the system. A snapshot of the liquid phase clearly indicates positional disorder and the presence of free disclinations (figure 11 (c)). The defect structures in these snapshots are consistent with the Halperin-Nelson theory of 2-d melting. Together, these results provide strong evidence of a liquid to a hexatic to a crystal transition in the individual layers of methane. However, we note that they do not provide concrete proof of the existence of the hexatic

phase, because of the relatively small size of our system. This would require a careful calculation of the free energy in the hexatic phases and a systematic finite size scaling analysis which we have not attempted here [40,41]. For our purpose, this study provides sufficient insight into the nature of the fluid phases in figures 3(a) & (b) and the reason for the weakly first order nature of the freezing transition.

3.4 Hysteresis

The irreversibility associated with the freezing and melting paths in a liquid to crystalline solid phase transition is a common feature, and is attributed to the existence of metastable states due to the presence of local minima in the free energy surface. In the case of the melting/freezing transition in the bulk, it is well known that the degree of supercooling (hysteresis associated with the freezing path) is usually much greater than the degree of superheating (hysteresis associated with the melting path) [42,43]. The source of this asymmetry can be described as follows: liquids crystallize by nucleation in the bulk phase or about an impurity, in a two step process. The first step involves the formation of a nucleus of the crystal phase of size greater than the critical nucleus, which is an activated process [44]; the second step involves the growth of the critical nucleus and can be described by a rate mechanism analogous to chemical reactions. On the other hand, the nucleation of the liquid phase during melting is easily accomplished by the process of surface melting. Crystals in the bulk have free surfaces. The amplitudes of vibration of the surface atoms are greater than those in the bulk. The Lindemann criterion [45,46] states that the solid melts when the root mean square deviation of the atomic positions from their lattice positions exceed 15% of the nearest neighbor distance. Therefore, the surface melts more easily, thereby nucleating the liquid phase. In some special cases the surface melting was carefully controlled to achieve a larger degree of supercooling, which supports the above reasoning [47,48].

Hysteresis associated with freezing/melting in confined systems is typically much greater in extent than in the bulk. The melting and freezing curves also appear to be more continuous (therefore, less first-order-like) in confined systems. Simulations in structured single pores [3,4] show the same characteristic behavior, suggesting that these features are present even in the absence of polydispersity in the pore sizes, and kinetic effects due to pore networking and bottle-necks. The greater degree of supercooling in confined systems is explained by the fact that the average pore size can be smaller than the size of the critical nucleus. Therefore, the system has to be cooled further to reduce the size of the critical nucleus below the pore width for the liquid to freeze [6]. The absence of free surfaces in a confined solid inhibits surface melting, leading to a greater degree of superheating.

The adsorption behavior for methane in graphite for two slightly different pore widths is shown in figure 12. Both systems have seven molecular layers of methane, yet the extent of hysteresis is much larger for the slightly smaller pore. The continuous nature of the freezing curves is explained by the evidence of a liquid to hexatic to crystal transition in each of the layers; these transitions take place at different temperatures for different layers, as discussed in section 3.3. Since each transition in a particular layer is associated with a small change in density, the overall freezing curve appears continuous in spite of the absence of polydispersity in our model. Regarding the extent of the hysteresis loops, Miyahara and Gubbins [3] hypothesized that the average distance between molecular layers in the pore plays a crucial role. As seen from figure 12, decreasing the interlayer separation Δ from $0.94\sigma_{ff}$ (for $H = 7.5\sigma_{ff}$ pore) to $0.91\sigma_{ff}$ (for $H = 7.2\sigma_{ff}$ pore) increases the width of the hysteresis loop from about $16K$ to about $34K$.

The Landau free energy results explain the shape of the adsorption curve for the case of the $7.5\sigma_{ff}$ graphite pore; comparing figure 6 and figure 12, it is evident that the liquid freezes completely around $T = 109K$, the temperature at which the Landau free energy

surface of Phase B becomes unstable (saddle point behavior). Similarly, at a temperature $T = 123K$, the Landau free energy surface for the crystal phase (Phase C) becomes unstable, and the crystal melts as seen from the melting curve. These calculations help to quantify the behavior of hysteresis loops, but do not provide any physical insight into the dependence of the local minima of the free energy surface on system parameters, or the nature of the metastable states. In this section, we use a simple one dimensional model to qualitatively understand the dependence of the hysteresis associated with melting on the inter-layer spacing in the graphite pore.

The in-plane, two-dimensional pair correlation function for the different layers are shown in figure 3b&c for the pore width $7.5\sigma_{ff}$ for temperatures $T = 123K$ and $101K$ respectively. At $T = 101K$, all the layers have the structure of a hexagonal crystal. However, at $T = 123K$ when the desorption (melting of the inner layers) occurs (see figure 12), the contact layers are frozen and the inner layers have an isotropic fluid structure. In the case of the more tightly packed layers for $H = 7.2\sigma_{ff}$, all the layers remain frozen even at $T = 123K$, as seen in figure 13 (a). However, when the desorption occurs at $T = 134K$, all the layers, including the contact layers, undergo melting and assume an isotropic structure (figure 13 (b)).

The melting within each layer is controlled by two kinds of effective potentials. One of them is the intermolecular potential due to other molecules in the same layer, and can be thought of as nearest neighbors within a layer connected by springs. The other potential is an effective substrate potential due to all other layers and the pore-wall, which is typically periodic (the potential surface shaped like an egg carton), since all the layers are frozen, as shown in figure 14. The amplitudes of vibrations of molecules within each layer are determined by the relative magnitudes of the spring constant (α) and the depth of the egg-carton potential (v_o). It is intuitive that for a given value of the spring constant, a deeper egg-carton potential will lead to lesser amplitudes of vibrations

within a layer. This is shown quantitatively for a one-dimensional model in the appendix (see also figure 17). This argument, together with the Lindemann criterion, leads to the conclusion that a layer experiencing a deeper egg-carton-like substrate potential would melt at a higher temperature than a layer experiencing a shallow substrate potential.

The spring constant within each layer is dependent on the fluid-fluid LJ parameters, and therefore is the same for all the layers and for both pore widths ($7.5\sigma_{ff}$ and $7.2\sigma_{ff}$); the general nature of the substrate potential is also the same, as indicated in figure 14. However, the depth of the substrate-potential wells (v_o) differ for the two pore widths, as seen from figure 15. The potential surface acting on a particular layer is calculated by summing over the fluid-fluid interactions from all molecules outside the layer, and adding the fluid-wall interaction. The negative of the substrate potential is plotted for the sake of easy visualization of the three dimensional surface. Therefore, the peaks in the plots actually correspond to the minima in the egg-carton potential. The contact layers for both pore widths experience a similar kind of potential surface (figures 15 (a)&(c)) due to the substrate, with a small value of v_o [49]. However, the potential surface for the layer adjacent to the contact layer is different for the two pore widths; v_o for the tightly packed layers is evidently greater than that for the loosely packed layers from figures 15 (b)&(d). Based on these observations, the contact layers for both pore widths are expected to melt at similar temperatures $T \geq 124K$ (the freezing point of the contact layers), but the inner layers in the smaller pore ($H = 7.2\sigma_{ff}$) would melt at a higher temperature compared to those in the larger pore ($H = 7.5\sigma_{ff}$), leading to a larger hysteresis loop in the case of the smaller pore. This is also consistent with the pair correlation function plots in figure 3 (b),(c) and figure 13.

In this interpretation, we have neglected the out-of-plane motion of molecules within a layer, and the effect of the melting of one layer on an adjacent layer. Nevertheless, the effect of inter-layer spacing on the hysteresis is explained qualitatively.

4 Conclusions

We have used the Landau free energy formalism to calculate the grand free energy of the fluid and crystalline states as a function of temperature, for LJ methane confined in slit-shaped pores. The free energy difference between the ordered and the disordered state is directly calculated, thereby eliminating the need to numerically integrate the free energy, starting from a well characterized reference phase. Thus, unlike the methods that involve thermodynamic integration, this method is not limited to repulsive or weakly attractive fluid-wall potentials. In addition to the free energy, this method provides quantitative information on the energy barrier to nucleation, although this is a quantity sensitive to system size effects and needs careful interpretation. However, the free energy difference is only a weak function of system size, and is estimated to an accuracy of $1k_BT$, as shown by Lynden-Bell *et al.* [14]. Our free energy results clearly indicate a first order fluid to crystal transition for methane confined in both hard wall and graphite pores. They also confirm the sensitivity of the shift in the freezing point to the nature of the fluid-wall potential [3], by calculating the exact temperatures at which the transitions occur. The exact location of the equilibrium transition temperature by free energy calculation is an improvement over methods that use the jump in the density to locate the freezing/melting points in terms of accuracy, as it is independent of the width of the hysteresis loops.

Methane confined in graphite shows strong evidence of a quasi-two-dimensional behavior, and our results indicate the occurrence of an intermediate hexatic phase between the fluid and crystal phases. The specific heat and structure factor calculations, and the analysis of defect structures, support the Halperin-Nelson theory of two-dimensional melting. These results also provide an explanation for the weak first order nature of the freezing transition, as most of the entropy change is believed to occur in the fluid-hexatic transition. A rigorous proof to the existence of the hexatic phase would involve a careful analysis of system size effects, which we have not attempted. The fluid-hexatic transi-

tion could be studied in more detail using the Landau free energy method by choosing a more appropriate order parameter. It may also be possible to directly observe the hexatic phase experimentally, using electron diffraction or equivalent techniques on fluids confined in graphite pores.

The Landau free energy method also provides a systematic procedure to relate the width of the hysteresis loops in our model system to features of the free energy surface. This route however, does not provide any physical insight into the dependence of the metastable states on system or model parameters. The hysteresis associated with the freezing and melting paths in the graphite pore is a strong function of the inter-layer separation. Tightly packed layers exert a periodic substrate potential with deep potential wells; this causes the melting of individual layers to occur at higher temperatures as a result of the suppression of the amplitudes of vibrations of the molecules in the layers, leading to larger hysteresis loops.

The extension of the free energy method to fluids confined in model cylindrical pores and other, more realistic, pore models that include poly-dispersity and pore networks would be of great practical interest. Such calculations would enable direct comparison with experimental data on freezing and melting in pores to be made. The key to such a study is finding a suitable order parameter that distinguishes between the ordered and disordered phases. We propose to undertake such a study in the future for porous glasses, and to make quantitative comparisons with experiment.

5 Acknowledgments

It is a pleasure to thank M. Sliwinska-Bartkowiak, K. Kaneko and M. Miyahara for helpful discussions, and R. Evans for sending his manuscript prior to publication. The work was supported by the National science foundation under Grant Nos. CTS-9712138

and INT-9511946, and by a Metacenter grant (No. MCA93S011P). We also thank the Cornell Theory center for providing the computing facilities.

6 References

1. R Evans, 1990, J.Phys.: Condensed matter, 2, 8989.
2. K.E. Gubbins, M. Sliwinska-Bartkowiak, and S.H. Suh, 1996, Mol. Simulation, 17, 333.
3. M. Miyahara, and K.E. Gubbins, 1997, J. Chem. Phys., 106(7), 2865.
4. M. Maddox, and K.E. Gubbins, 1997, J. Chem. Phys., 107(22), 9659.
5. H. Dominguez, M.P. Allen, and R. Evans, 1998, Mol. Phys., in press.
6. J. Warnock, D.D. Awschalom, and M.W. Shafer, 1986, Phys. Rev. Lett., 57, 1753.
7. K.M. Unruh, T.E. Huber, and C.A. Huber, 1993, Phys. Rev. B, 48, 9021.
8. J. Klein, and E. Kumacheva, 1995, Science,269, 816.
9. M.A. Castro, S.M. Clarke, A. Inaba, and R.K. Thomas, 1997, J. Phys. Chem. B, 101, 8878.
10. D. Nicholson, and N.G. Parsonage, 1982, Computer simulation and the statistical mechanics of adsorption, (London: Academic Press).
11. R. Evans, and U.M.B. Marconi, 1987, J. Chem. Phys., 86, 7138.
12. D. Frenkel, and A.J.C. Ladd, 1984, J. Chem. Phys, 81 (7), 3188.
13. The fluid phase referred to here, is characterized by a frozen contact layer but is liquid-like in the interior of the pore.
14. R.M. Lynden-Bell, J.S. van Duijneveldt, and D. Frenkel, 1993, Mol. Phys, 80 (4), 801.
15. W.A. Steele, 1973, Surf. Sci. 36, 317.

16. W.A. Steele, 1974, The interaction of gases with solid surfaces, (Oxford: Pergamon press).

17. S. Jiang, and K.E. Gubbins, 1993, Mol. Phys., 80, 103.

18. Woods G.B., and Rowlinson J.S., 1989, J. Chem. Soc., Faraday Trans., 2, 85 756.

19. L.D. Landau, and E.M. Lifshitz, 1980, Statistical Physics., 3rd edn. (London:Pergamon Press).

20. P.M. Chaikin, and T.C. Lubensky, 1995, Principles of Condensed Matter Physics, (Cambridge: Cambridge University Press).

21. J.S. van Duijneveldt, and D. Frenkel, 1992, J. Chem. Phys., 96 (6), 4655.

22. G.M. Torrie, and J.P. Valleau, 1974, Chem. Phys. Lett., 28, 578.

23. J.K. Johnson, J.A. Zollweg, and K.E. Gubbins, 1993, Mol. Phys., 78, 3, 591.

24. D.A. Kofke, 1993, J. Chem. Phys., 98, 4149.

25. R. Agrawal, and D.A. Kofke, 1995, Mol. Phys., 85, 43.

26. P.J. Steinhardt, D.R. Nelson, and M. Ronchetti, 1983, Phys. Rev. B, 28, 784.

27. We note that the Landau free energy formalism is independent of any arbitrariness involved in the definition of the order parameter such as choosing of the nearest neighbor cutoff distance r_{nn}.

28. C.G. Gray, and K.E. Gubbins, 1984, Theory of Molecular Liquids, (Oxford: Clarendon Press), App. A.

29. L.D. Landau, and E.M. Lifshitz, 1965, Quantum Mechanics, (NewYork: Pergamon press).

30. J.P. Hansen, and L. Verlet, 1969, Phys. Rev., 184, 151; S. Ranganathan, and K.N. Pathak, 1992, Phys. Rev. A, 45, 5789.

31. N.D. Mermin, 1968, Phys. Rev., 176, 250.

32. B.I Halperin, and D.R. Nelson, 1978, Phys. Rev. Lett., 41, 121; D.R. Nelson, and B.I. Halperin, 1979, Phys. Rev. B., 19, 2457; A.P. Young, 1979, Phys. Rev. B, 19, 1855.

33. N. Goldenfeld, 1992, Lectures on Phase Transitions and the Renormalization group, (Addison-Wesley).

34. N.D. Mermin, and H. Wagner, 1966, Phys. Rev. Lett., 17, 1133.

35. J.M. Kosterlitz, and D.J. Thouless, 1972, J. Phys. C, 5, L124; J.M. Kosterlitz, and D.J. Thouless, 1973, J. Phys. C, 6, 1181.

36. K.J. Strandburg, 1988, Rev. Mod. Phys., 60, 161; K.J. Strandburg, 1989, Rev. Mod. Phys., 61, 747; K.J. Strandburg (editor), 1992, Bond Orientational Order in Condensed Matter Systems, (NY: Springer-Verlag).

37. J.D. Brock, R.J. Birgeneau, J.D. Lister, and A. Aharony, 1989, Physics Today, July, 52.

38. R.J. Birgeneau, and J.D. Lister, 1978, J. de Physique Letters, 39, L399.

39. C.Y. Chao, C.F. Chou, J.T. Ho, S.W. Hui, A. Jin, and C.C. Huang, 1996, Phys. Rev. Lett., 77, (13), 2750.

40. J. Lee, and J.M. Kosterlitz, 1990, Phys. Rev. Lett., 65, 2, 137.

41. V. Privman (editor), 1990, Finite Size Scaling and Numerical Simulation of Statistical Systems, (World Scientific).

42. D.W. Oxtoby, 1990, Nature, 347, 725.

43. D. Frenkel, and J.P. McTague, 1980, Ann. Rev. Phys. Chem., 31, 491.

44. D.W. Oxtoby, 1988, Adv. Chem. Phys., 70,2, 263.

45. F.A. Lindemann, 1910, Z. Phys., 11, 609.

46. M. Baus, 1987, J. Statistical Phys., 48, 1129.

47. D. Dages, H. Gleiter, and J.H. Perepezko, 1987, Materials Res. Soc. Symp. Proc., 57, 67.

48. A. D. J. Haymet, 1987, Ann. Rev. Phys. Chem., 38, 89.

49. Although the value of v_o is small for the contact layers, there is a large contribution from the additional background attractive potential due to the pore walls.

A Appendix

Consider a one dimensional array of N atoms separated by a lattice spacing a. The inter atomic potential between these atoms is modeled as a harmonic potential (equivalent to the nearest neighbors being connected by springs).

$$v_{harmonic} \;=\; \frac{1}{2}\alpha(x_1 - x_2 - a)^2 \tag{1}$$

$v_{harmonic}$ is the harmonic potential between two nearest neighbors at coordinates x_1 and x_2. In addition, the line of atoms feel a periodic external potential $v_{substrate}$, due to a substrate which is a fixed row of atoms in an other layer.

$$v_{substrate} \;=\; -\frac{v_o}{2\pi}\cos\left(\frac{2\pi x}{a}\right) \tag{2}$$

The equilibrium structure of the row of atoms are shown in figure 16a. If there is a fluctuation that causes the configuration to look like figure 16b, then the fluctuation will relax to a final configuration that depends on the relative strengths of the harmonic and the substrate potential. Assuming that the relaxed configuration is according to figure 16c where there are a total of $N+1$ atoms of which n atoms redistribute to have a mean separation $a^* = na/(n+1)$ and the remaining $N-n$ atoms are undisturbed, the difference in total energy between the relaxed excited state and the equilibrium state is given by,

$$\Delta E \;=\; \Delta E_{harmonic} \;+\; \Delta E_{substrate} \tag{3}$$

where

$$\Delta E_{harmonic} \;=\; \frac{(n+1)\alpha}{2}\left(1 - \frac{n}{n+1}\right)^2 a^2 \tag{4}$$

and

$$\Delta E_{substrate} \;=\; \left[\sum_{k=1}^{n}\left(-\frac{v_o}{2\pi}\right)\cos\left(\frac{2\pi nk}{n+1}\right)\right] \;-\; \left(-\frac{(n-1)v_o}{2\pi}\right) \tag{5}$$

which on simplification yields,

$$\Delta E_{harmonic} \;=\; \frac{\alpha a^2}{2(n+1)} \;+\; \frac{nv_o}{2\pi} \tag{6}$$

Neglecting entropic effects, the configuration in the relaxed state is given by minimizing the change in total energy, $\frac{d(\Delta E)}{dn} = 0$, which gives

$$n \sim \left(\frac{\alpha a^2 \pi}{v_o}\right)^{1/2} \tag{7}$$

The root mean square deviation can be related to the quantity n, given that the nature of the fluctuation is as described above.

$$\left\langle \Delta r^2 \right\rangle = \frac{1}{N} \sum_{i=1}^{N} \left(r_i - \langle r_i \rangle\right)^2 \tag{8}$$

For the n disturbed atoms,

$$r_i = i\left(\frac{na}{n+1}\right) \text{ and } \langle r_i \rangle = ia \tag{9}$$

Substituting equation (9) into equation (8) yields,

$$\left\langle \Delta r^2 \right\rangle^{1/2} = \left(\frac{a^2}{6N}\right)^{1/2} \left(\frac{n(2n+1)}{n+1}\right)^{1/2} \tag{10}$$

The variation of the average root mean square displacement as a function of v_o can be determined from equation (7) and equation (10) and is plotted in figure 17.

List of Tables

Crystal	Q_4	Q_6	W_4	W_6	$\Phi = Q_6 - 3W_4$
f.c.c.	0.191	0.571	-0.159	-0.013	1.052
h.c.p.	0.097	0.485	0.134	-0.012	0.082
b.c.c.	0.036	0.511	0.159	0.013	0.033
s.c.	0.764	0.354	0.159	0.013	-0.124
Icosahedral	0	0.663	0	-0.170	0.663
Liquid	0	0	0	0	0

Most stable phase	Temperature range
Phase A	$T \geq 124K$
Phase B	$114K \leq T \leq 124K$
Phase C	$T \leq 114K$

List of Figures

1. Reproduced from Ref. [3]. The adsorption curves for LJ methane in slit shaped pores of pore width $7.5\sigma_{ff}$ for three different wall potentials showing the freezing of methane on cooling. For comparison, the dotted vertical line at $T = 101K$ represents the freezing of LJ methane in the bulk. The graphite wall represents an attractive fluid-wall potential, the hard wall represents a purely repulsive fluid-wall potential and the methane wall represents the case where the fluid-wall potential is roughly the same as the fluid-fluid potential.

2. Density profile of methane in the graphite pore along the direction perpendicular to the pore walls for four different temperatures showing distinct layering. The solid curve for $T = 101K$ is for the crystalline methane and is not symmetric about the center of the pore along the z axis because of defects in the two-dimensional crystal phase in the second and third layers. The profiles for the other temperatures correspond to a fluid phase and are symmetric.

3. The two-dimensional, in-plane pair correlation function for each of the layers for the $H = 7.5\sigma_{ff}$ graphite pore at three different temperatures: (a) $T = 130K$, corresponding to Phase A; (b) $T = 123K$, corresponding to Phase B; (c) $T = 101K$ corresponding to Phase C. Only 4 of the 7 layers are shown because of the symmetry about the mid-plane.

4. The Landau free energy as a function of the order parameter $\Phi = Q_6 - 3W_4$ for methane confined in a hard wall pore of $H = 7.5\sigma_{ff}$ for (a) $T = 60K$ and (b) $T = 45K$.

5. The grand free energy of the liquid and the crystal phases as a function of temperature for the hard wall system. The cross over point near $T_f = 48K$ determines the thermodynamic transition temperature.

6. The Landau free energy as a function of the order parameter, for methane confined in a graphite pore of pore width $7.5\sigma_{ff}$ for (a) $T = 123K$, (a) $T = 118K$, (b) $T = 113K$ and (d) $T = 109K$.

7. The grand free energy of the three phases A, B and C, as a function of temperature for the graphite pore. The cross over points $T_{A\text{-}B}$ and $T_{B\text{-}C}$ correspond to the two first order phase transitions.

8. Heat capacity of the whole system and the order parameter in the individual layers as a function of temperature as the system is cooled, for the graphite pore. These plots are not expected to be reversible during the heating sequence because of strong hysteresis effects.

9. The structure factor $I(k_x, k_y)$ (k_x, k_y being measured in nm^{-1}) for the first or contact layer in the graphite pore at, (a) $T = 160K$, (b) $T = 128K$, (c) $T = 111K$, (d) $T = 101K$.

10. The structure factor $I(k_x, k_y)$ (k_x, k_y being measured in nm^{-1}), for the third layer in the graphite pore at, (a) $T = 160K$, (b) $T = 128K$, (c) $T = 111K$, (d) $T = 101K$.

11. Snapshots of molecular configurations in the contact layer showing the defect structures in (a) Crystal phase ($T = 101K$), (b) hexatic phase ($T = 128K$) and (c) liquid phase ($T = 160K$).

12. The freezing and melting curves, showing the number of molecules adsorbed in the system as a function of temperature for two pore widths, $H = 7.5\sigma_{ff}$ and $H = 7.2\sigma_{ff}$. A slight change in the pore width causes a large change in the hysteresis behavior. The adsorption and desorption paths are along the solid-fluid co-existence line for the bulk.

13. The two-dimensional, in-plane pair correlation function for each of the layers for the $H = 7.2\sigma_{ff}$ graphite pore at two different temperatures: (a) $T = 123K$,

(b) $T = 134K$.

14. A contour plot of the substrate potential typically experienced by a layer calculated from a single snapshot during the GCMC simulation of the confined solid phase, showing the egg-carton-like, periodic nature of the potential surface. The coordinates x and y (plotted in arbitrary units), form the plane of the layer experiencing this potential. The distance between two adjacent minima roughly equal σ_{ff}.

15. A three dimensional plot of the negative substrate potential surface (where x and y are the coordinates forming the plane of the layers) for: (a) The contact layers in the larger pore $H = 7.5\sigma_{ff}$; (b) inner layers in the $H = 7.5\sigma_{ff}$ pore; (c) contact layers in the smaller pore $H = 7.2\sigma_{ff}$, (d) inner layers in the $H = 7.2\sigma_{ff}$ pore. The substrate potential is calculated using a single snap shot rather than averaging over configurations, and hence is not strictly periodic.

16. The configuration of the row of atoms and the egg-carton like substrate potential are shown. (a) Equilibrium configuration where the atoms occupy the positions corresponding to the minima in the substrate potential. (b) A fluctuation in which a extra atom is inserted. (c) The fluctuation relaxes through re-distribution of the positions of n of the atoms. We assume that the remaining $N - n$ atoms are undisturbed.

17. The root mean square displacement in units of the lattice spacing a as a function of v_o measured in units of $\alpha a^2 \pi$, as described by equation (10).

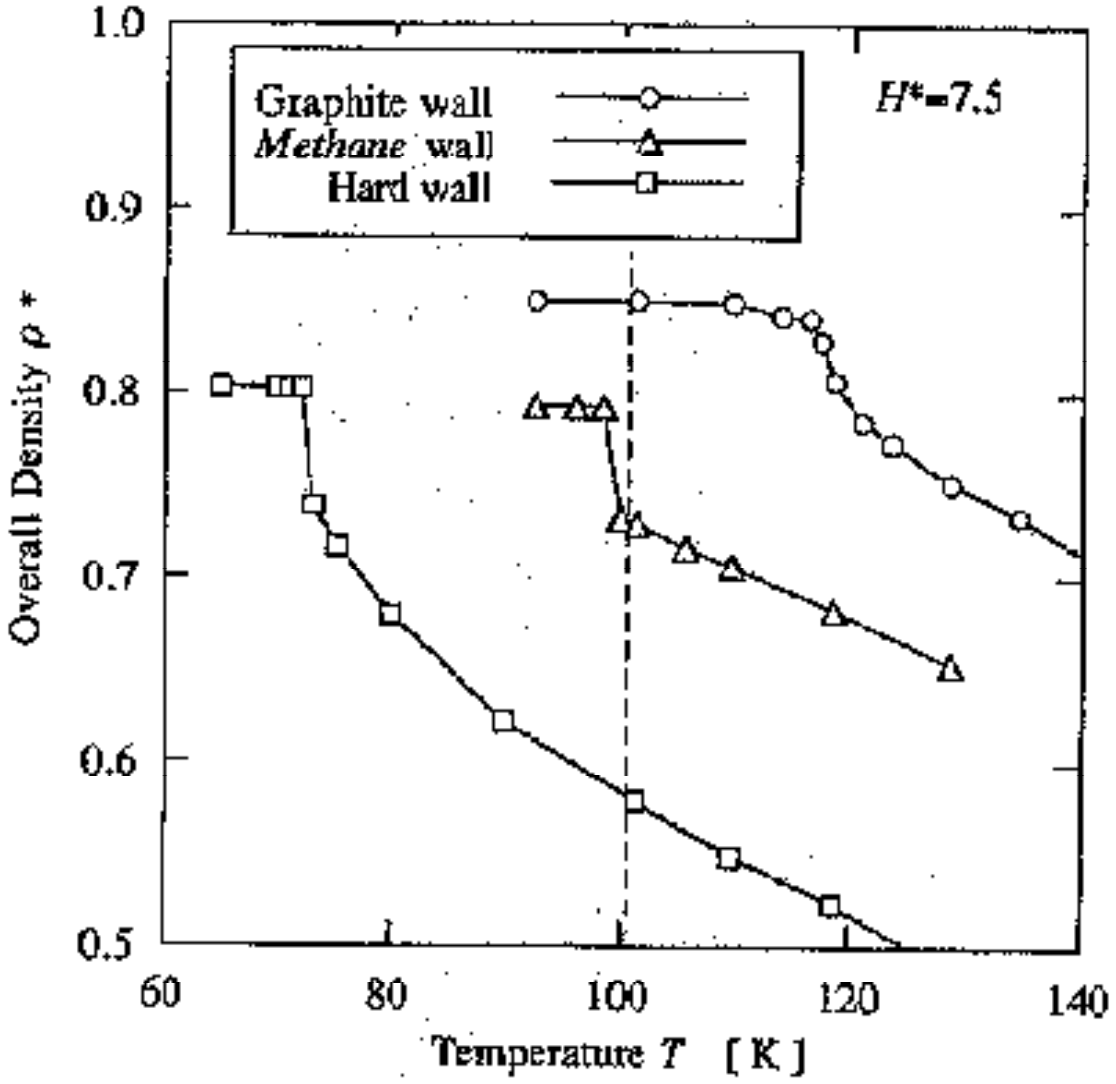
Graphite wall
Methane wall
Hard wall
H*=7.5
Overall Density ρ *
1.0
0.9
0.8
0.7
0.6
0.5
60
80
100
120
140
Temperature T [K]

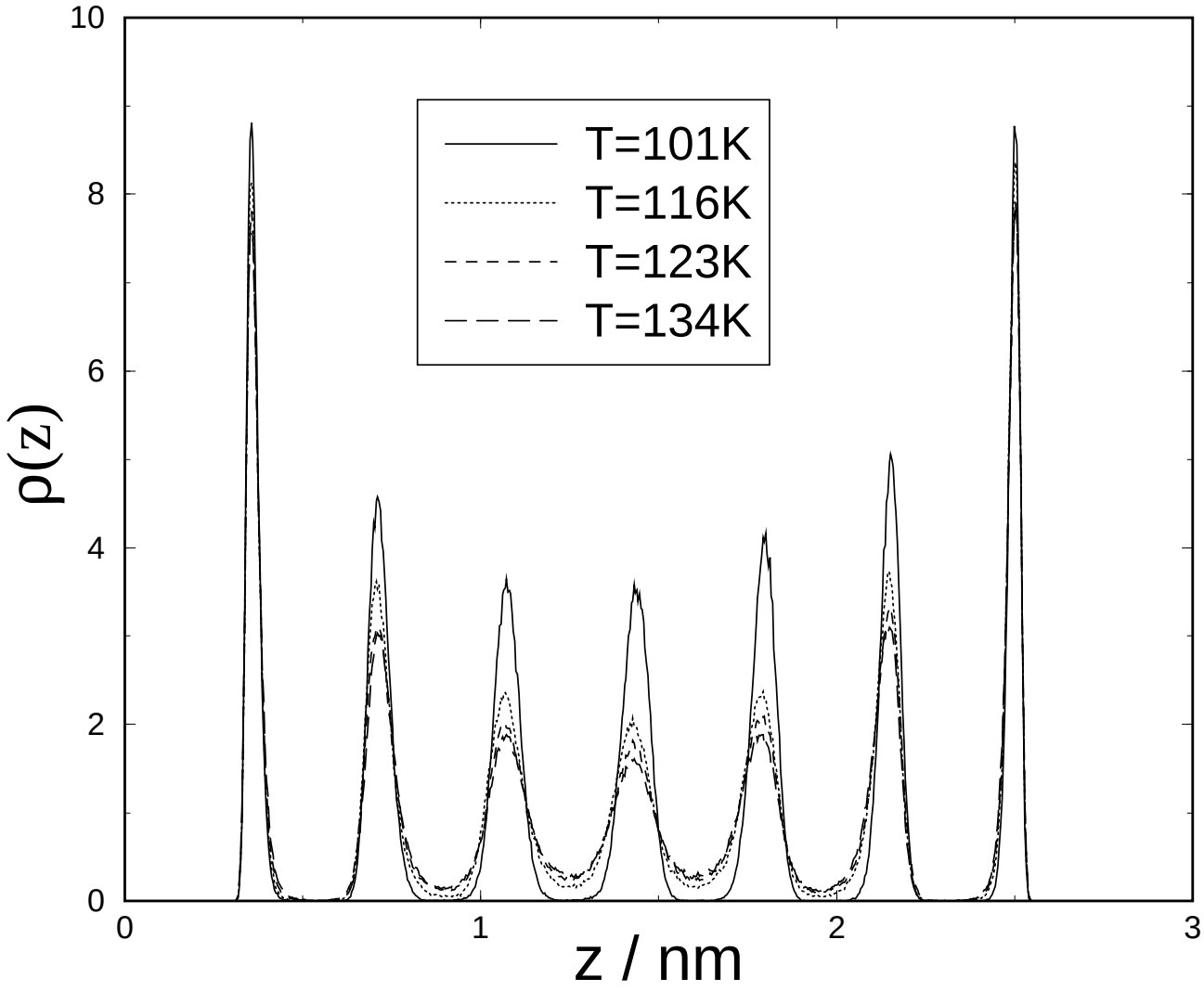
T=101K
T=116K
T=123K
T=134K
ρ(z)
z / nm
0
2
4
6
8
10
0
1
2
3

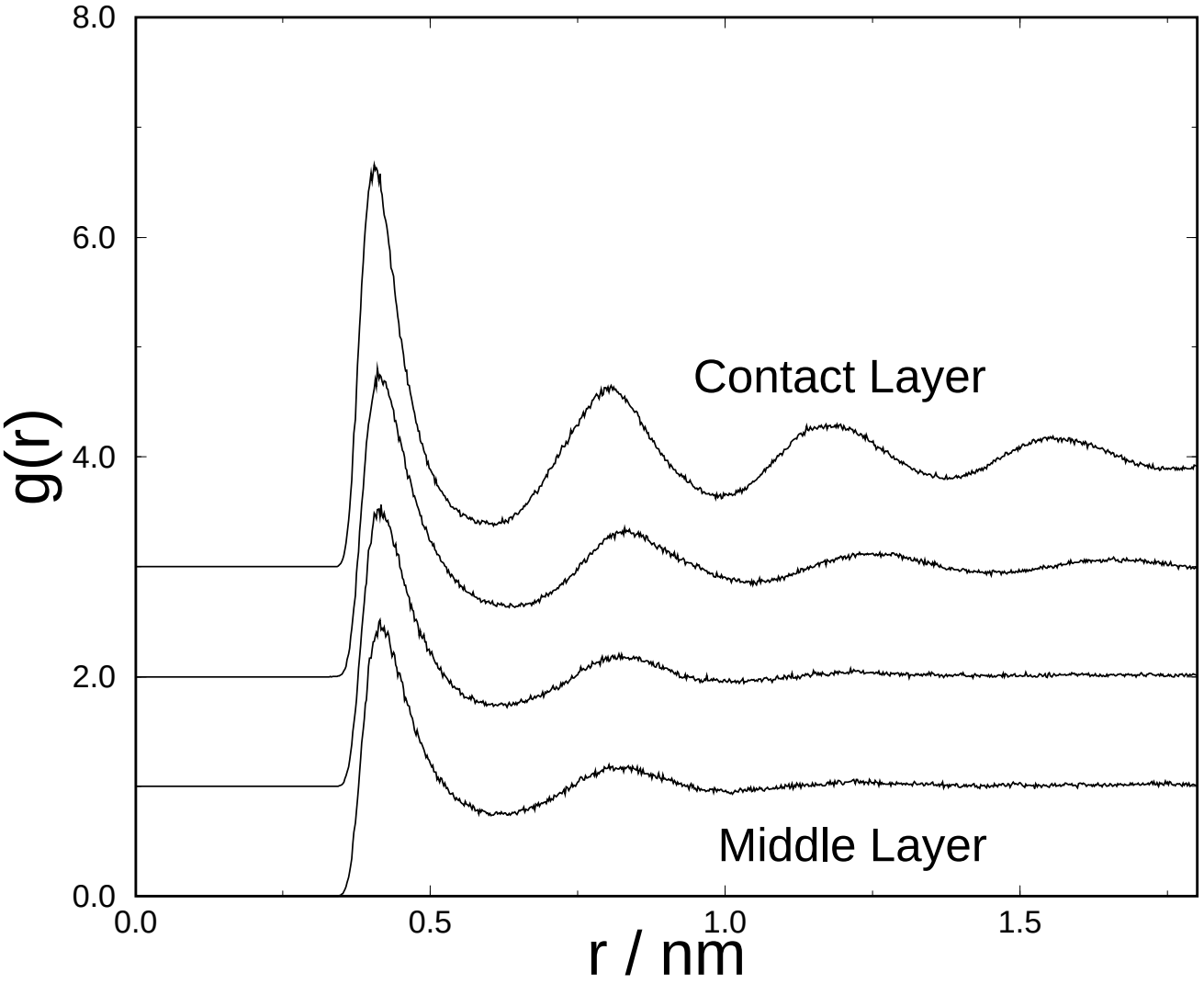
8.0
6.0
4.0
2.0
0.0
g(r)
0.0
0.5
1.0
1.5
r / nm
Contact Layer
Middle Layer

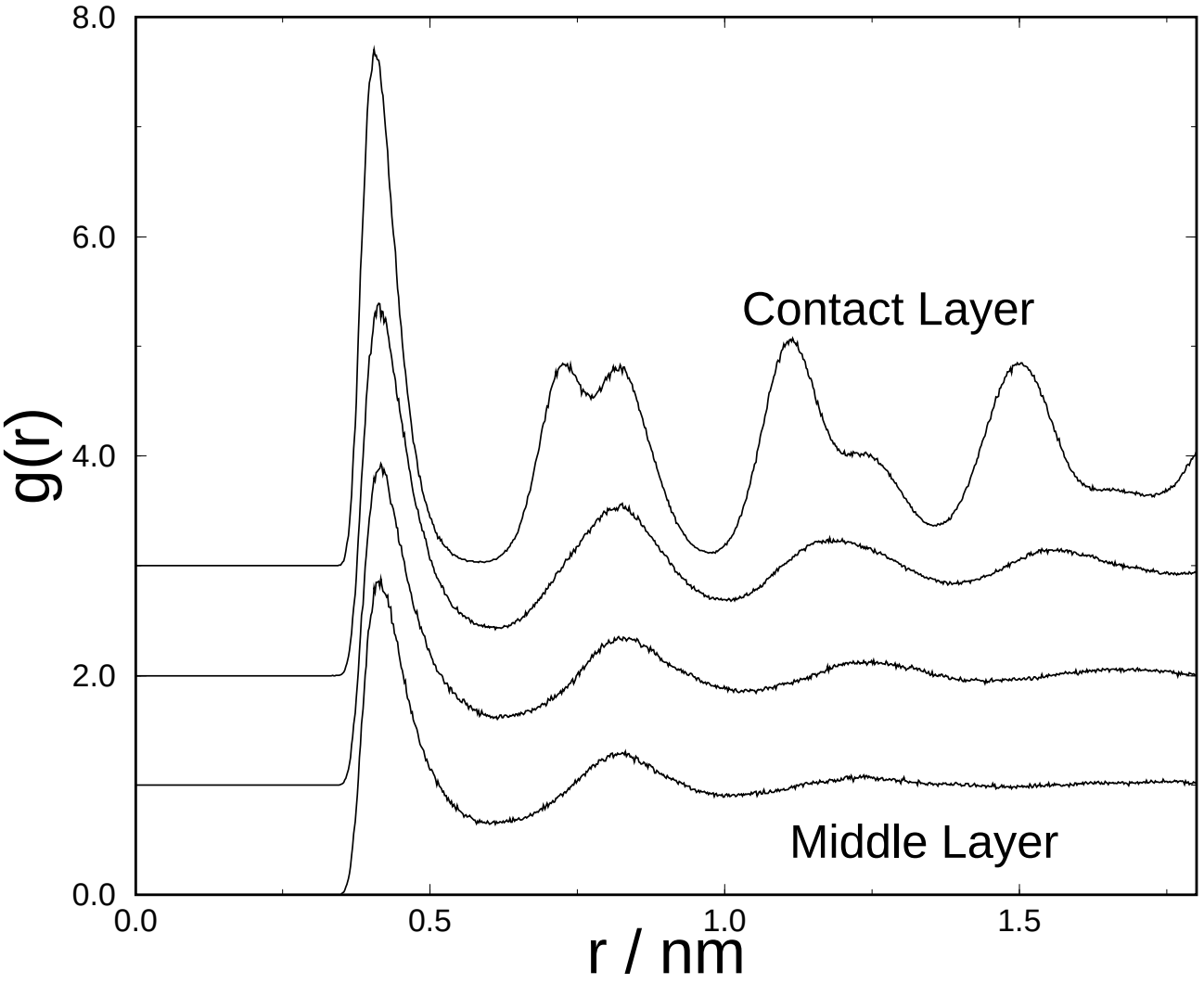
8.0
6.0
4.0
2.0
0.0
g(r)
0.0
0.5
1.0
1.5
r / nm
Contact Layer
Middle Layer

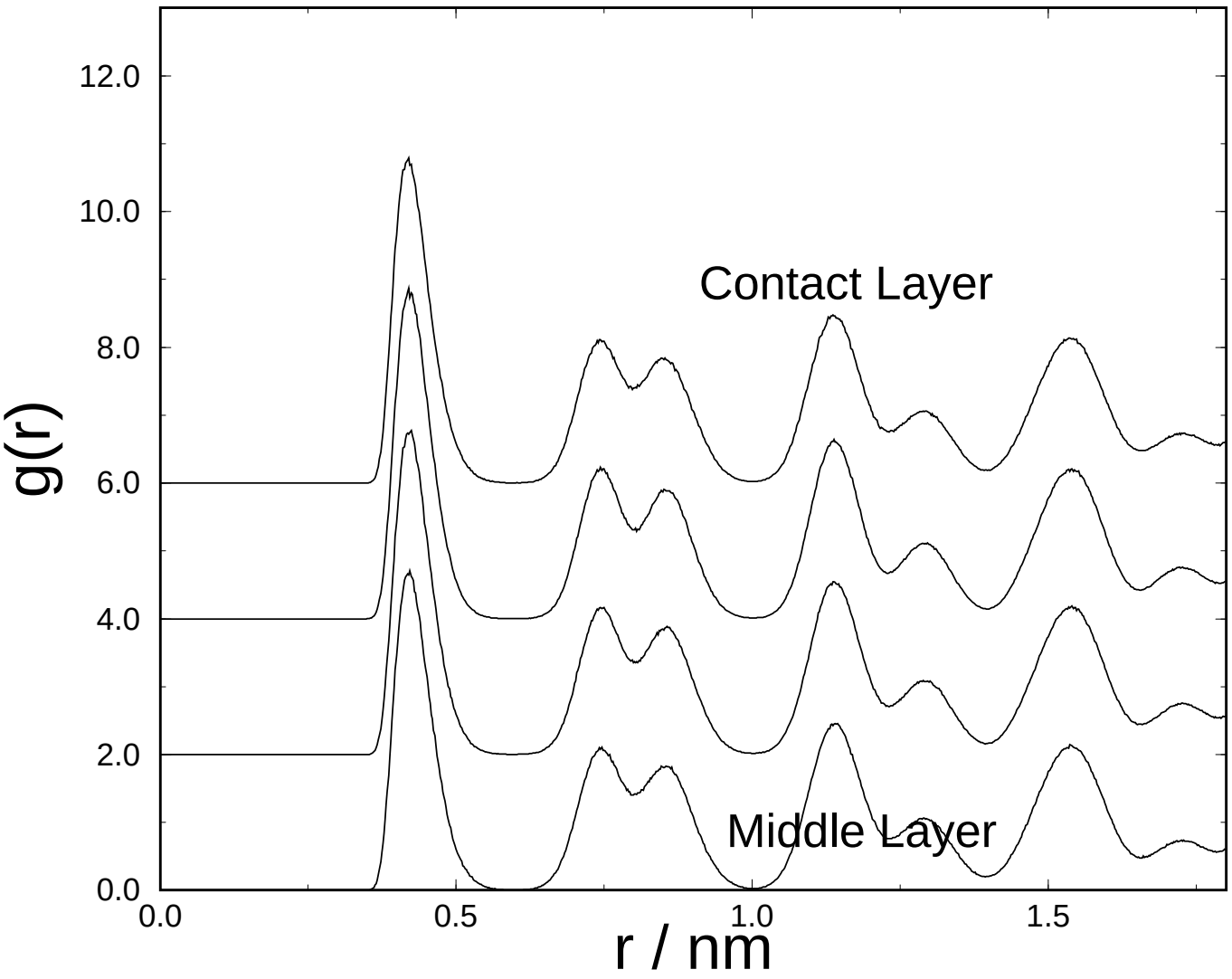
12.0
10.0
8.0
6.0
4.0
2.0
0.0
g(r)
Contact Layer
Middle Layer
0.0
0.5
1.0
1.5
r / nm

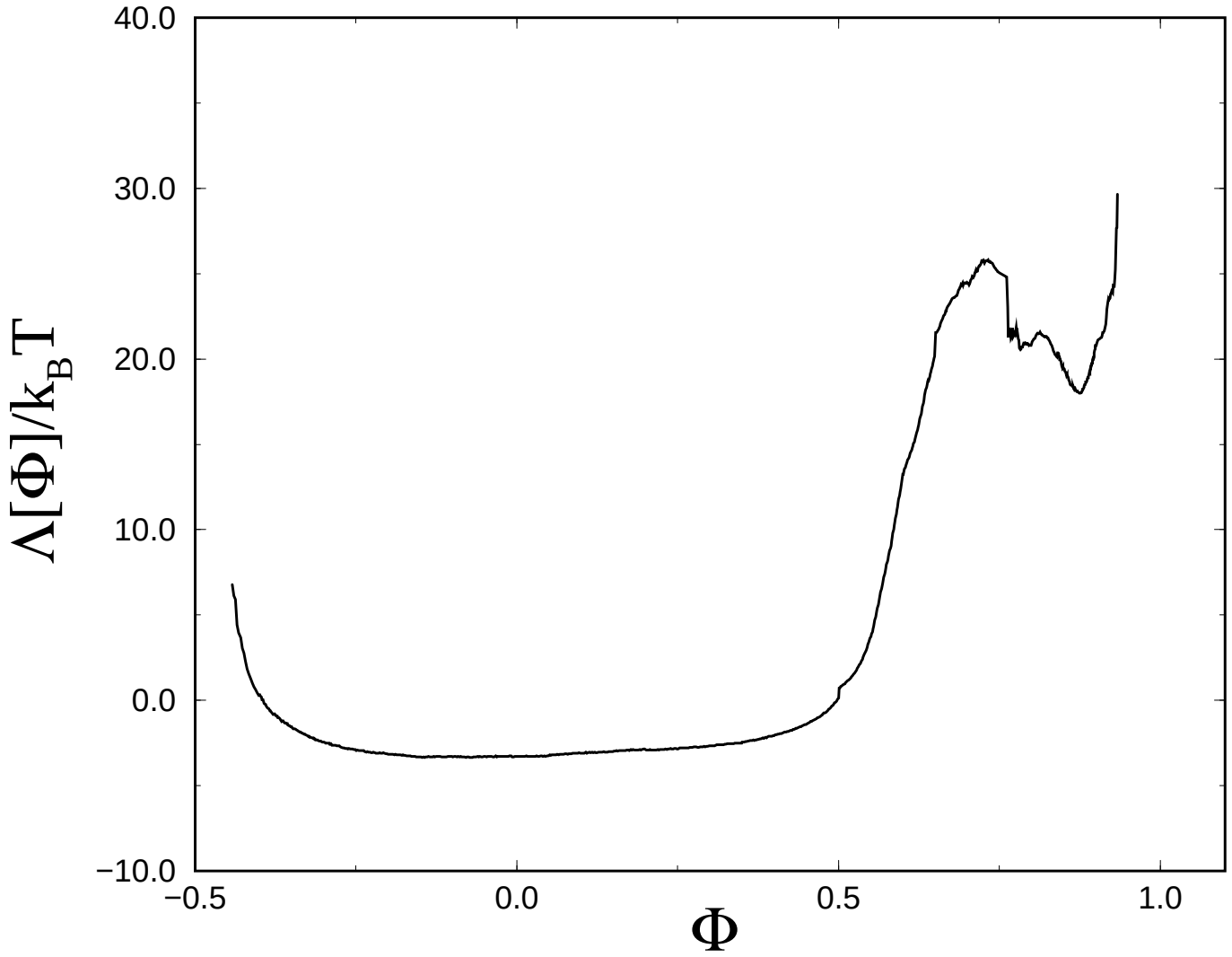
40.0
30.0
20.0
10.0
0.0
−10.0
−0.5
0.0
0.5
1.0
Φ
Λ[Φ]/k_BT

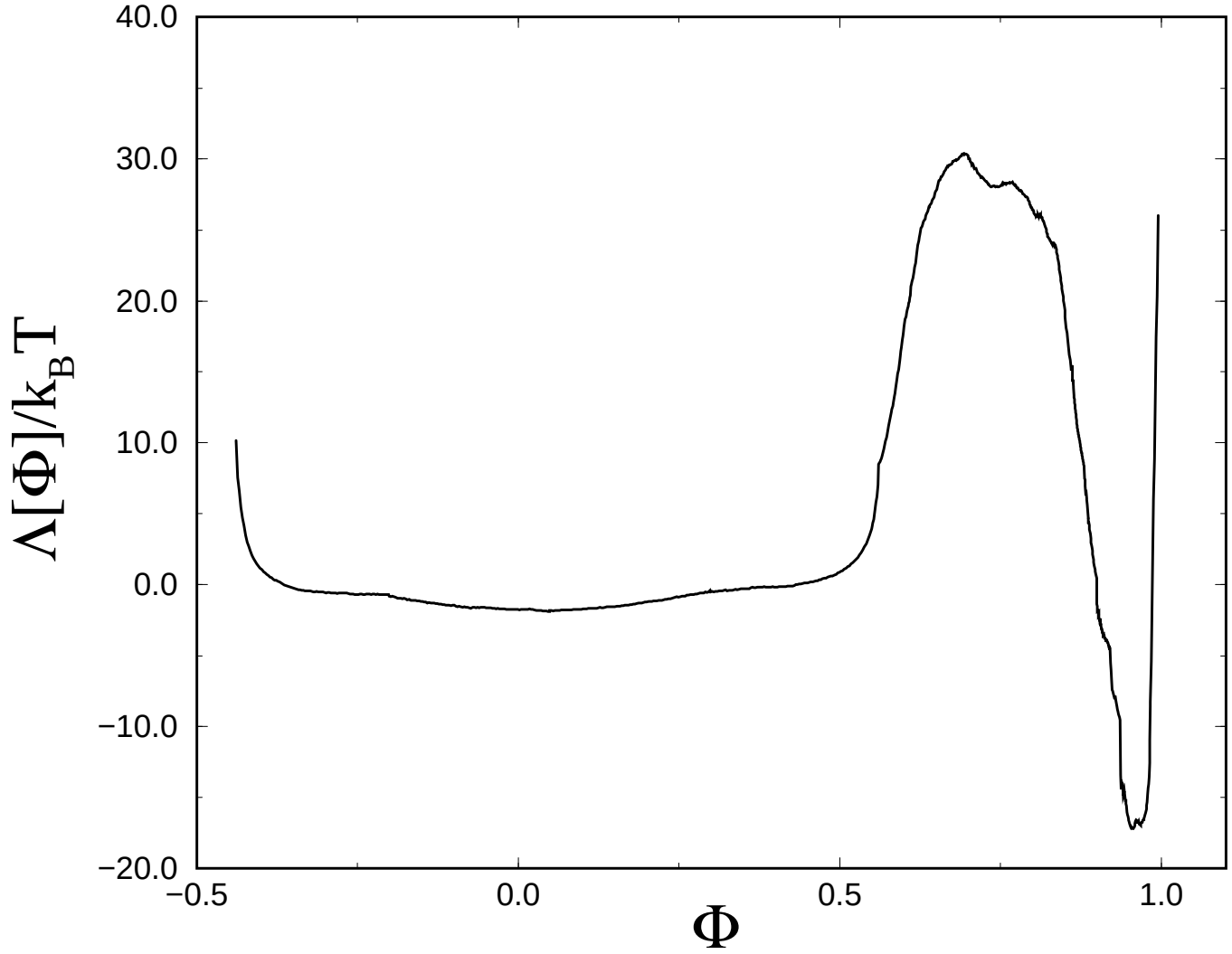
40.0
30.0
20.0
10.0
0.0
−10.0
−20.0
−0.5
0.0
0.5
1.0
Λ[Φ]/k_BT
Φ

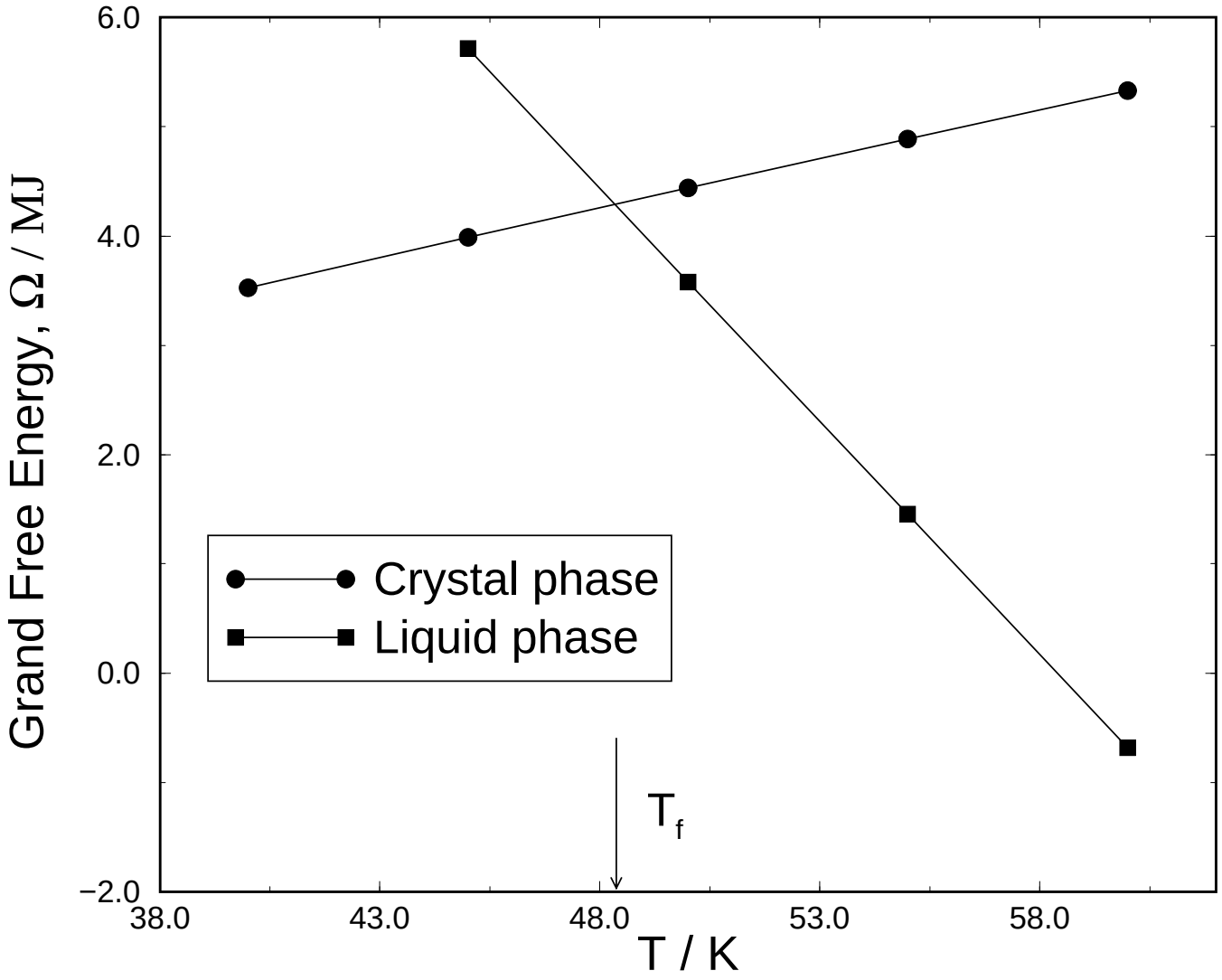
6.0
4.0
2.0
0.0
−2.0
38.0
43.0
48.0
53.0
58.0
Grand Free Energy, Ω / MJ
T / K
Crystal phase
Liquid phase
T_f

(a)

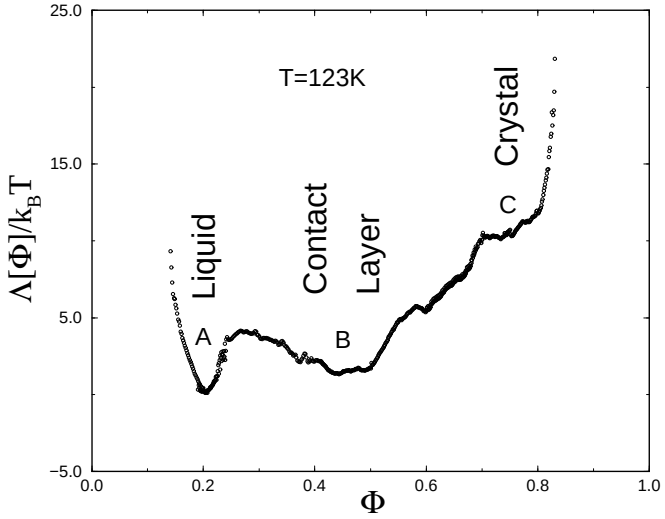
T=123K
Liquid
Contact
Layer
Crystal
A
B
C
$\Lambda[\Phi]/k_BT$
Φ

(b)

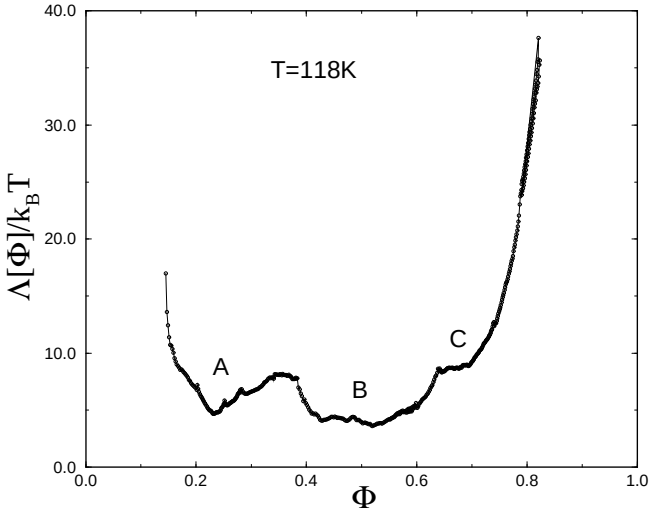
T=118K
A
B
C
$\Lambda[\Phi]/k_BT$
Φ

(c)

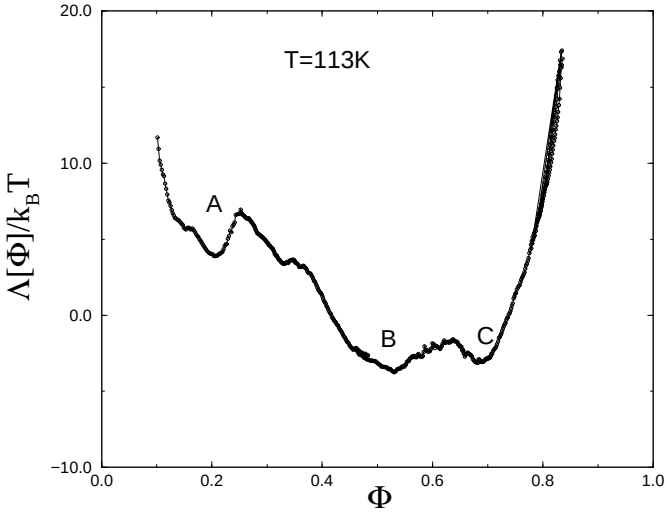
T=113K
A
B
C
$\Lambda[\Phi]/k_BT$
Φ

(d)

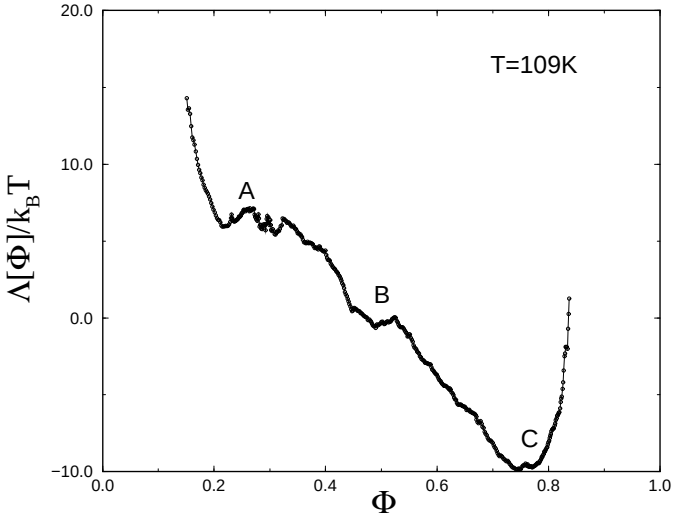
T=109K
A
B
C
$\Lambda[\Phi]/k_BT$
Φ

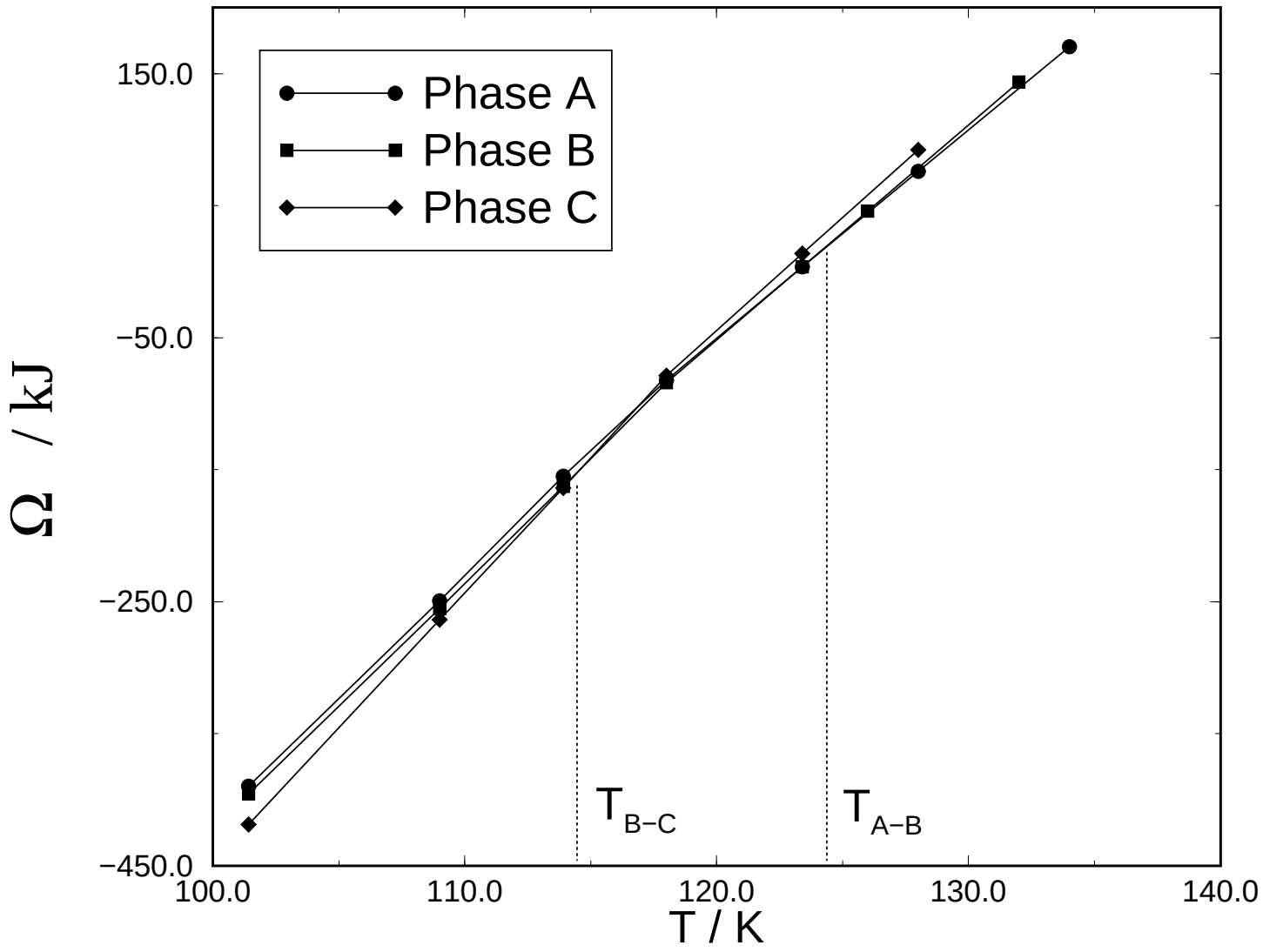
Phase A
Phase B
Phase C
150.0
−50.0
−250.0
−450.0
Ω / kJ
100.0
110.0
120.0
130.0
140.0
T / K
T B−C
T A−B

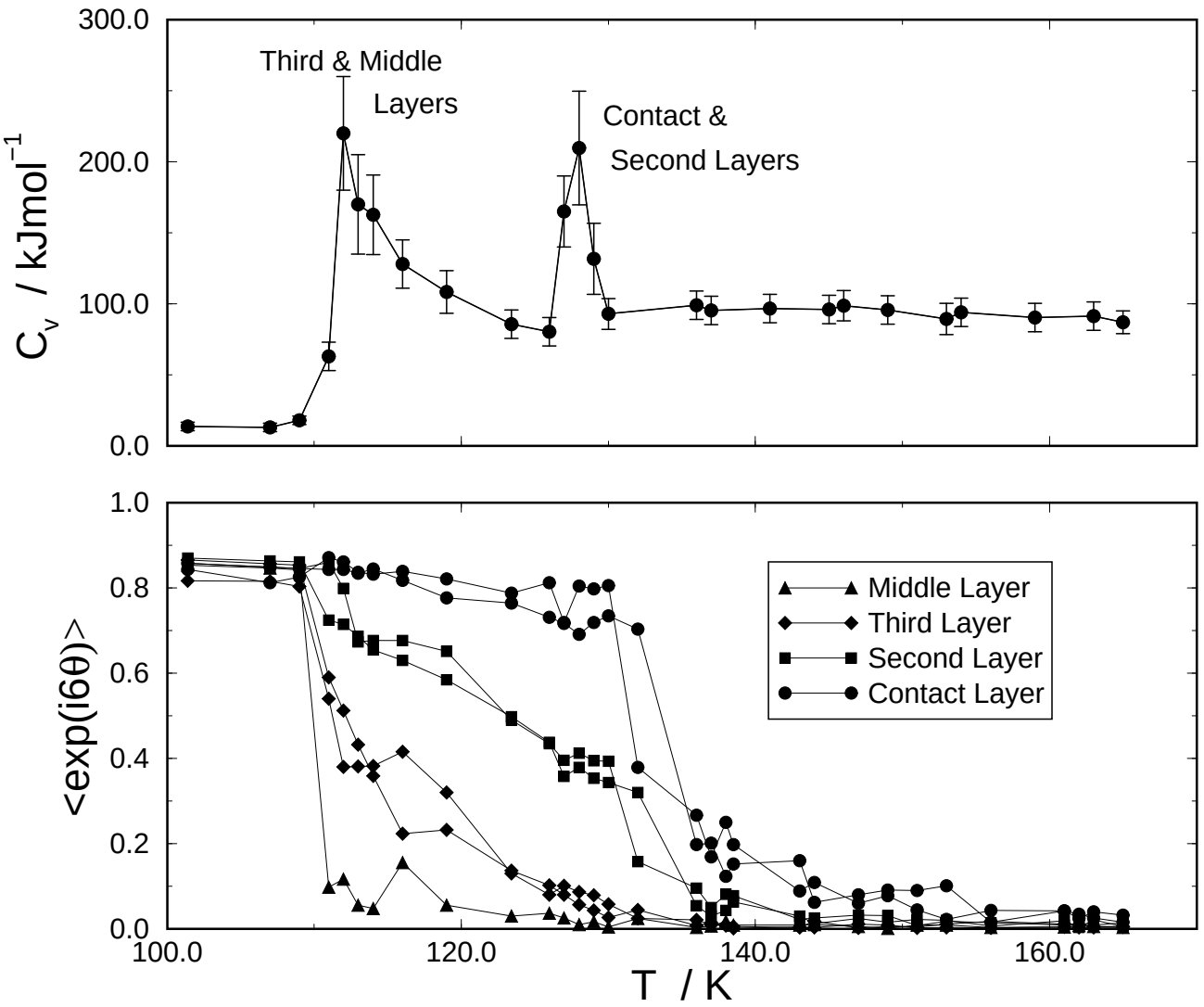
300.0
200.0
100.0
0.0
C_v / kJmol^{-1}
Third & Middle
Layers
Contact &
Second Layers
1.0
0.8
0.6
0.4
0.2
0.0
<exp(i6θ)>
Middle Layer
Third Layer
Second Layer
Contact Layer
100.0
120.0
140.0
160.0
T / K

(a)

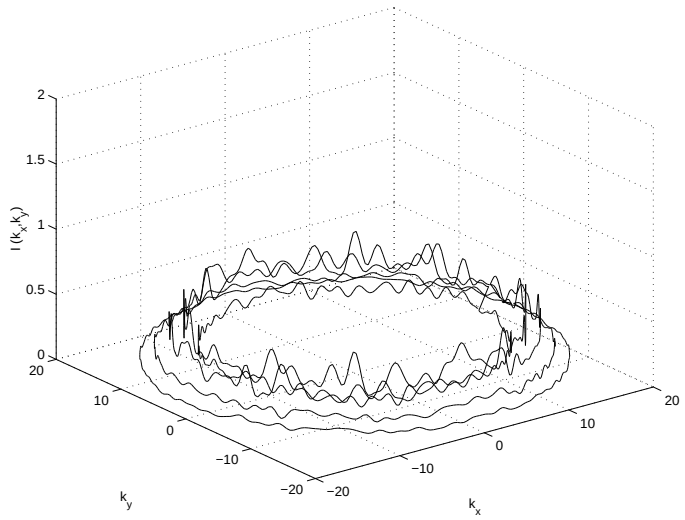

(b)

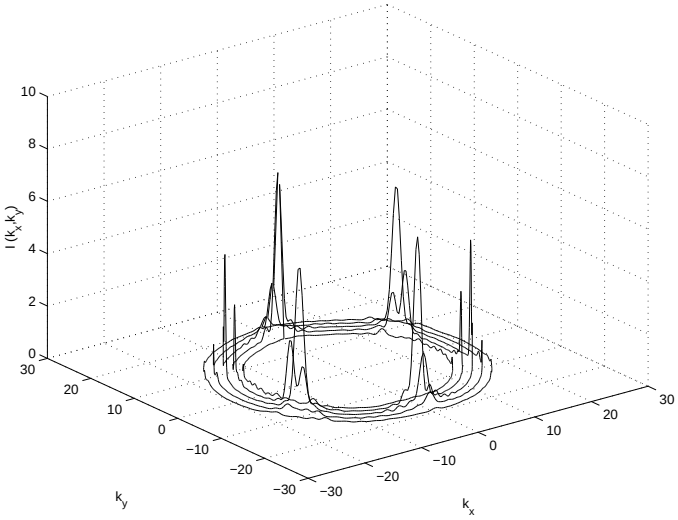

(c)

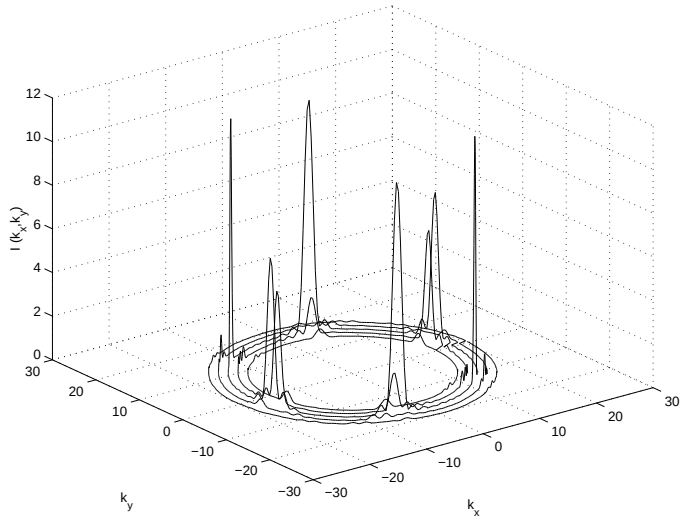

(d)

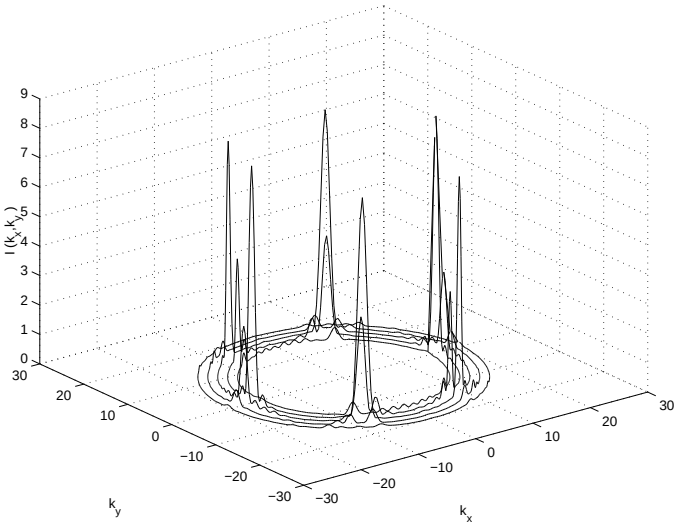

(a)

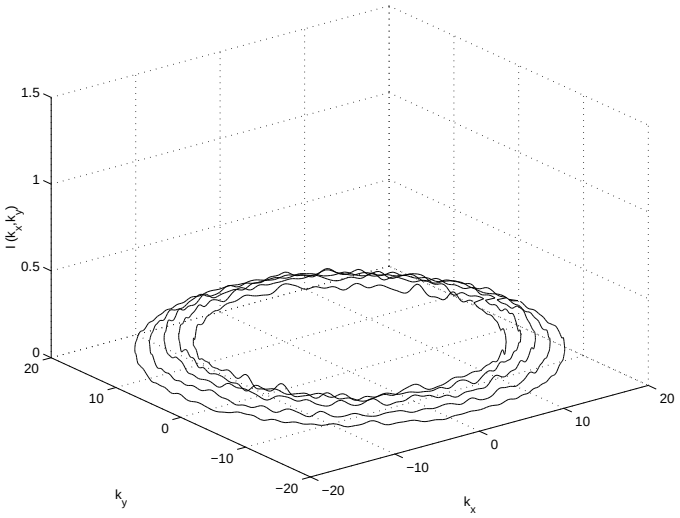

(b)

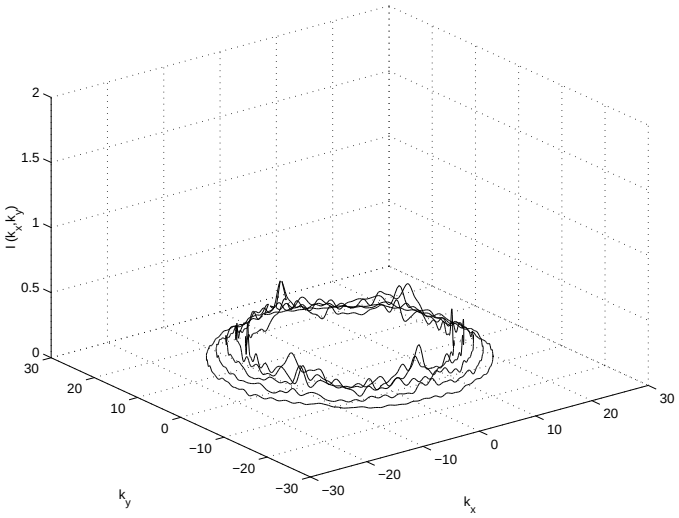

(c)

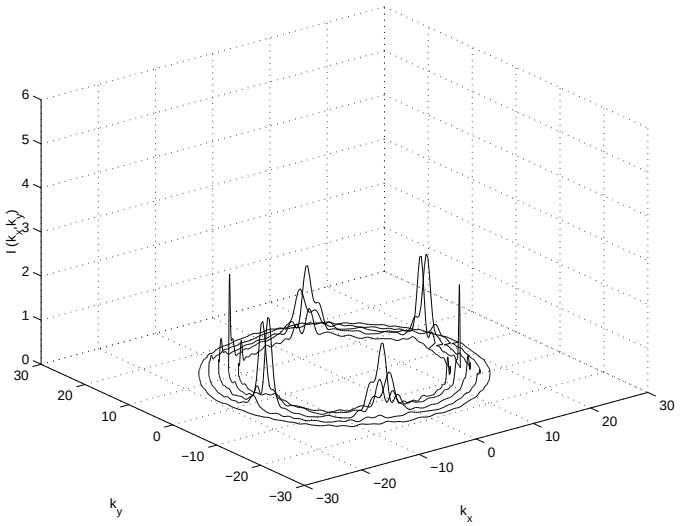

(d)

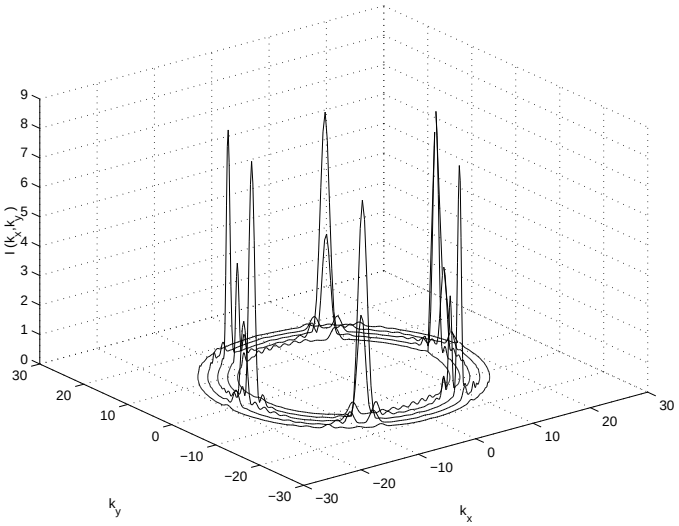

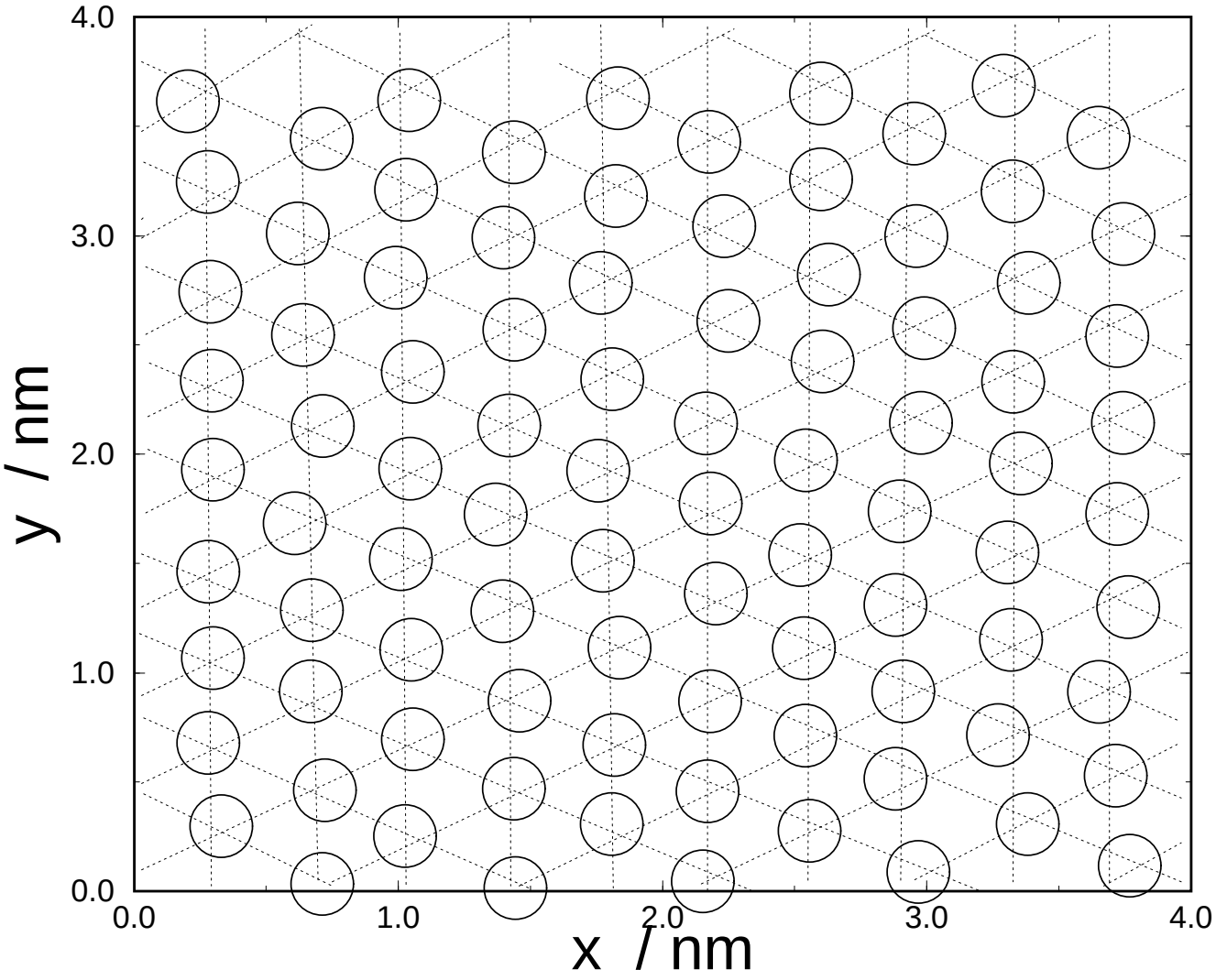
4.0
3.0
2.0
1.0
0.0
y / nm
0.0
1.0
2.0
3.0
4.0
x / nm

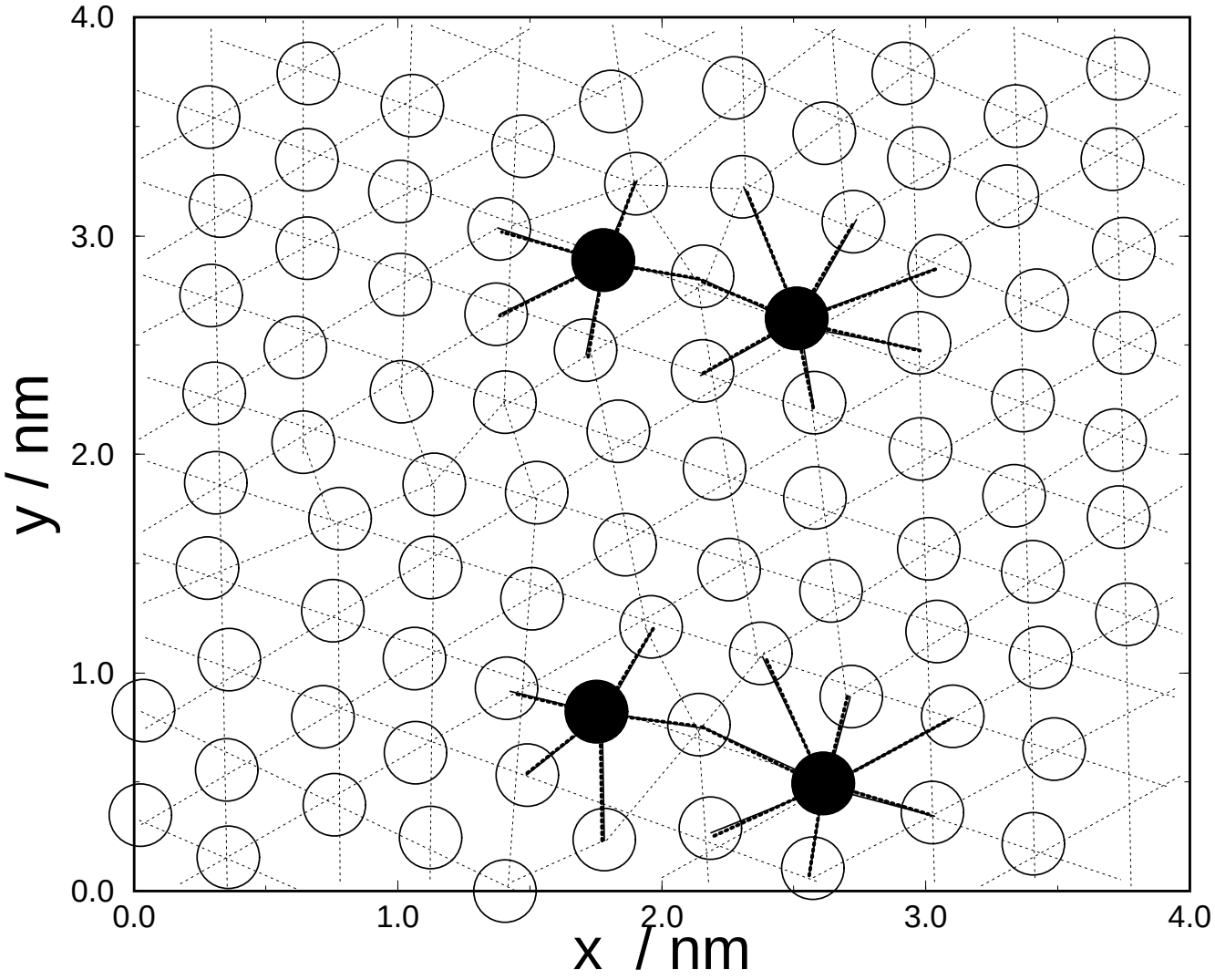
4.0
3.0
2.0
1.0
0.0
y / nm
0.0
1.0
2.0
3.0
4.0
x / nm

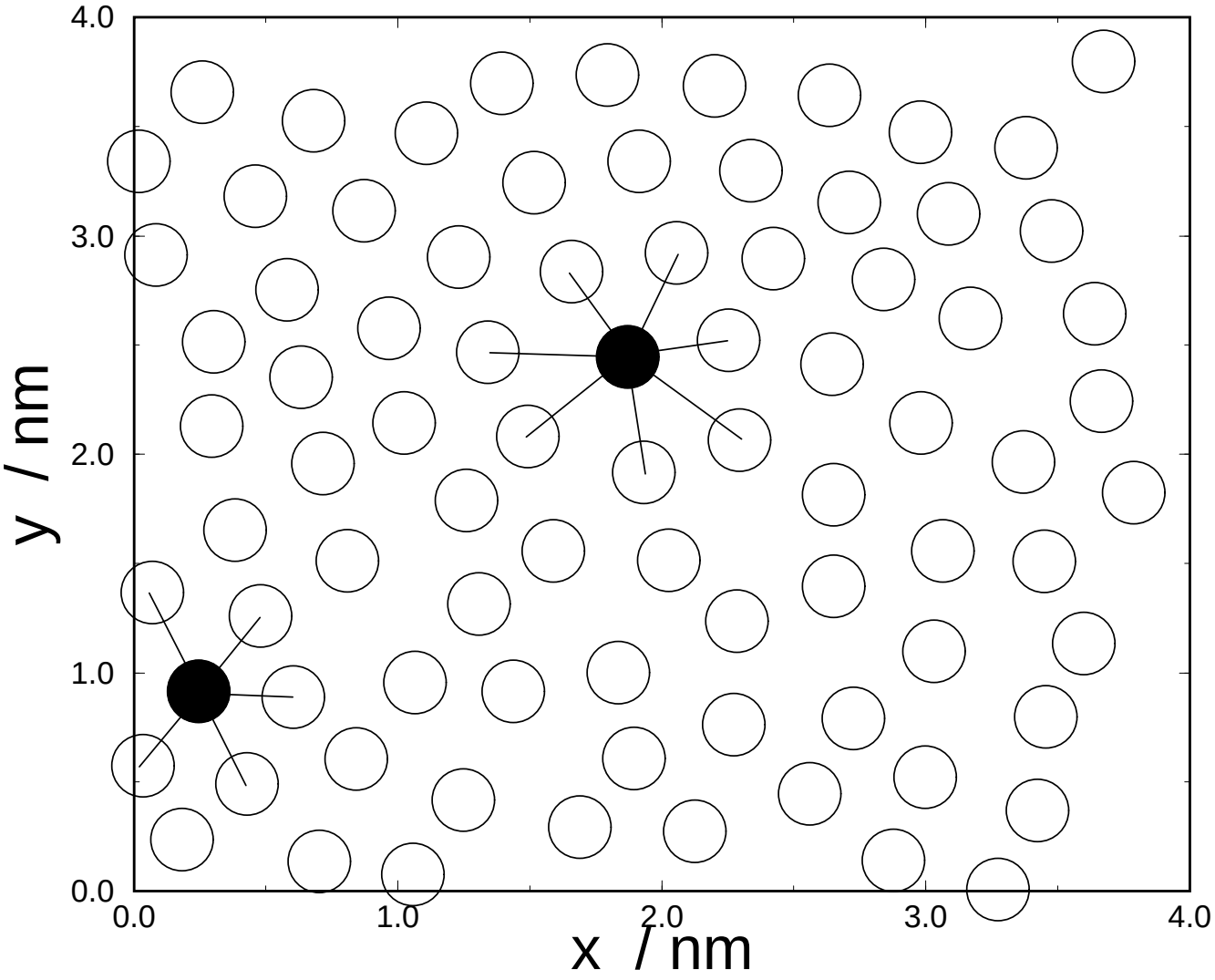
4.0
3.0
2.0
1.0
0.0
y / nm
0.0
1.0
2.0
3.0
4.0
x / nm

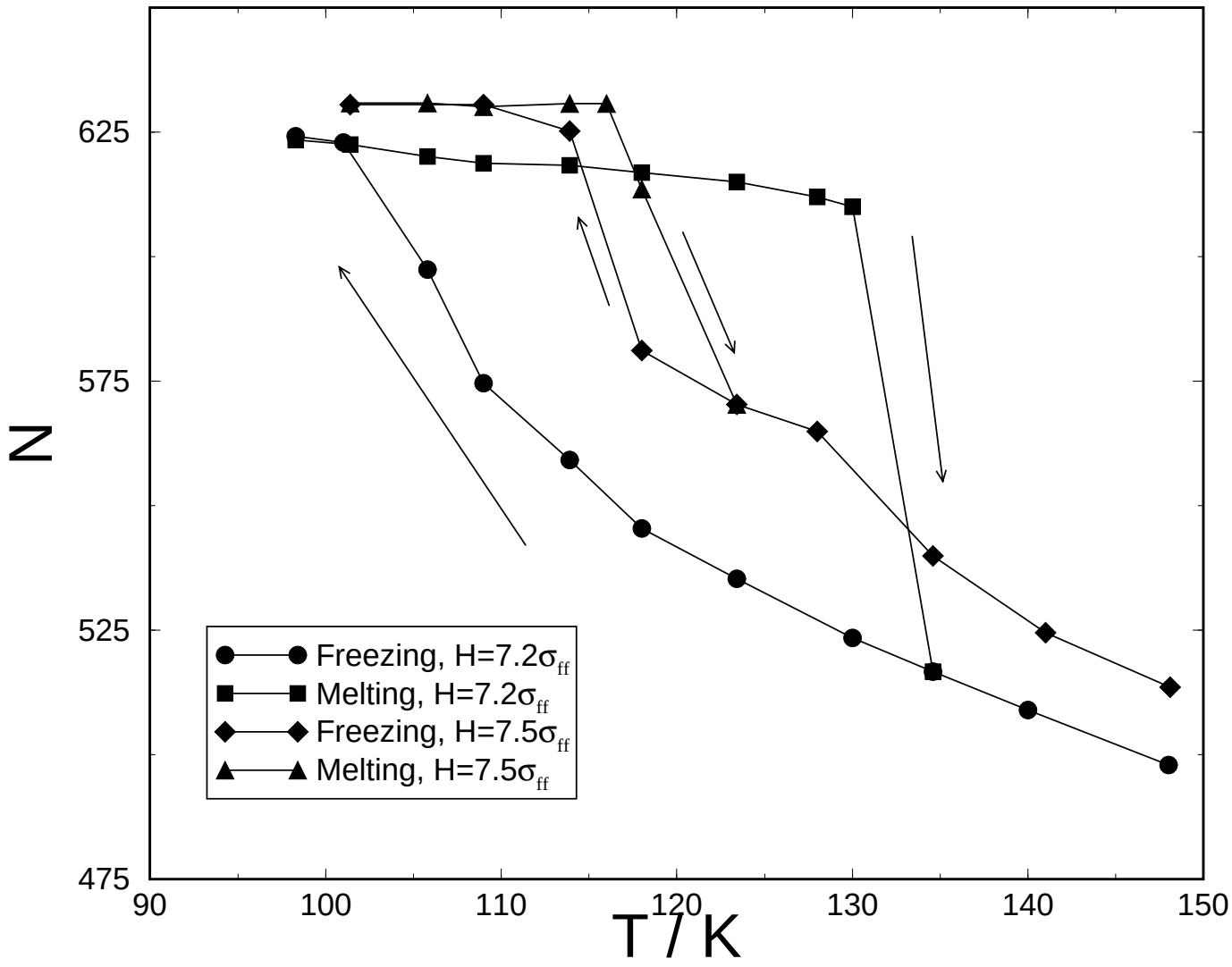
625
575
525
475
90
100
110
120
130
140
150
N
T / K
Freezing, H=7.2σff
Melting, H=7.2σff
Freezing, H=7.5σff
Melting, H=7.5σff

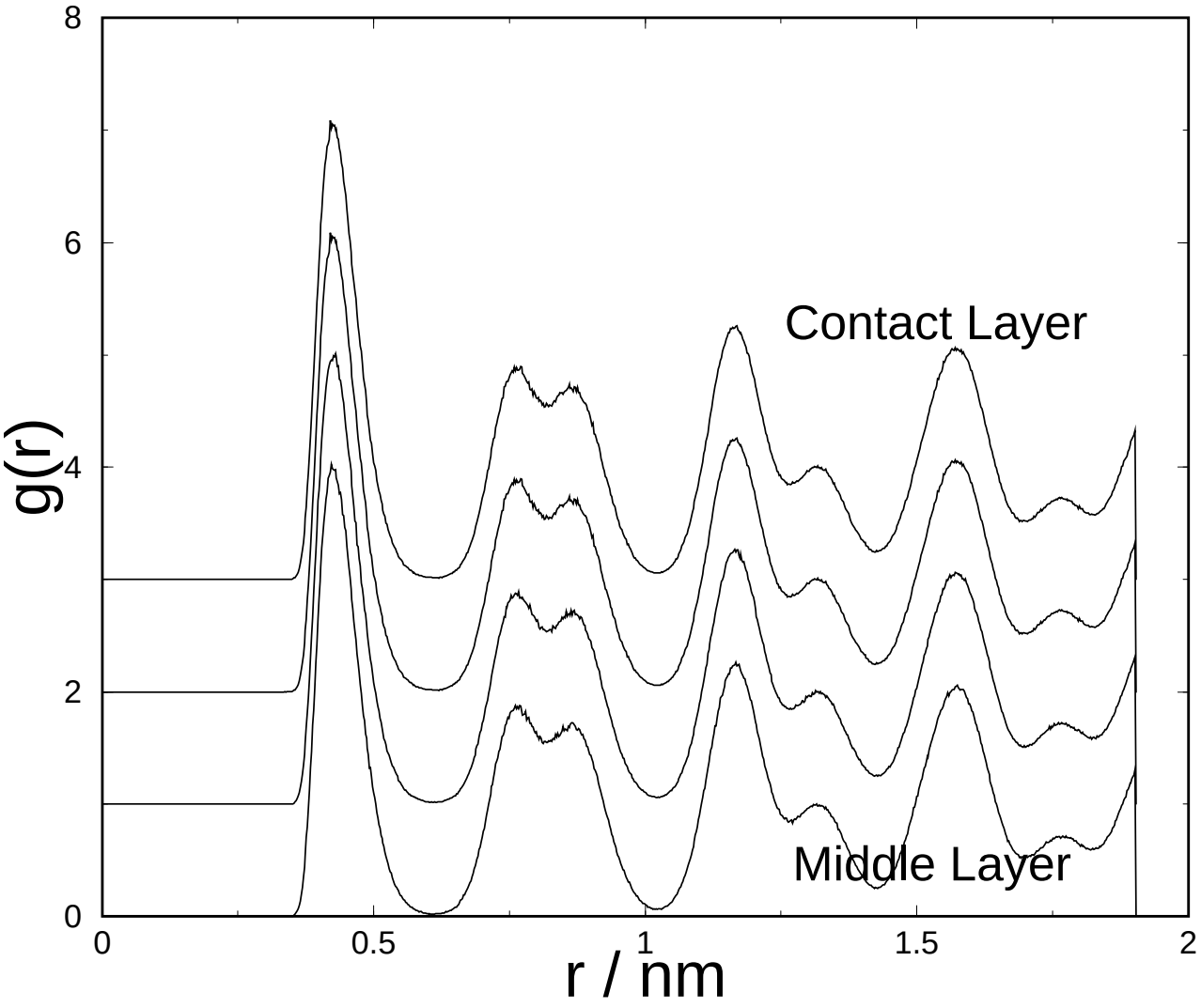
8
6
4
2
0
g(r)
0
0.5
1
1.5
2
r / nm
Contact Layer
Middle Layer

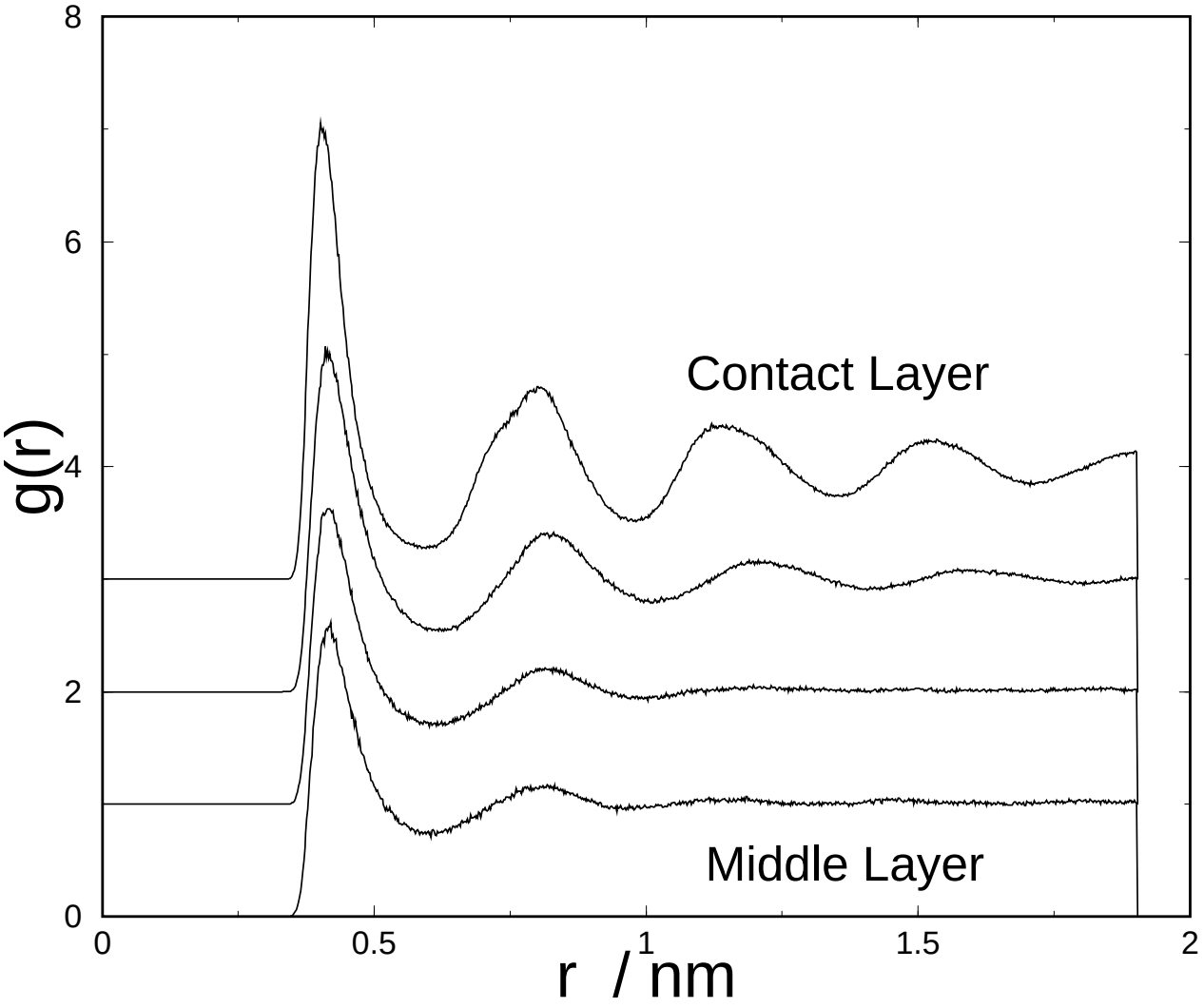
8
6
4
2
0
g(r)
Contact Layer
Middle Layer
0
0.5
1
1.5
2
r / nm

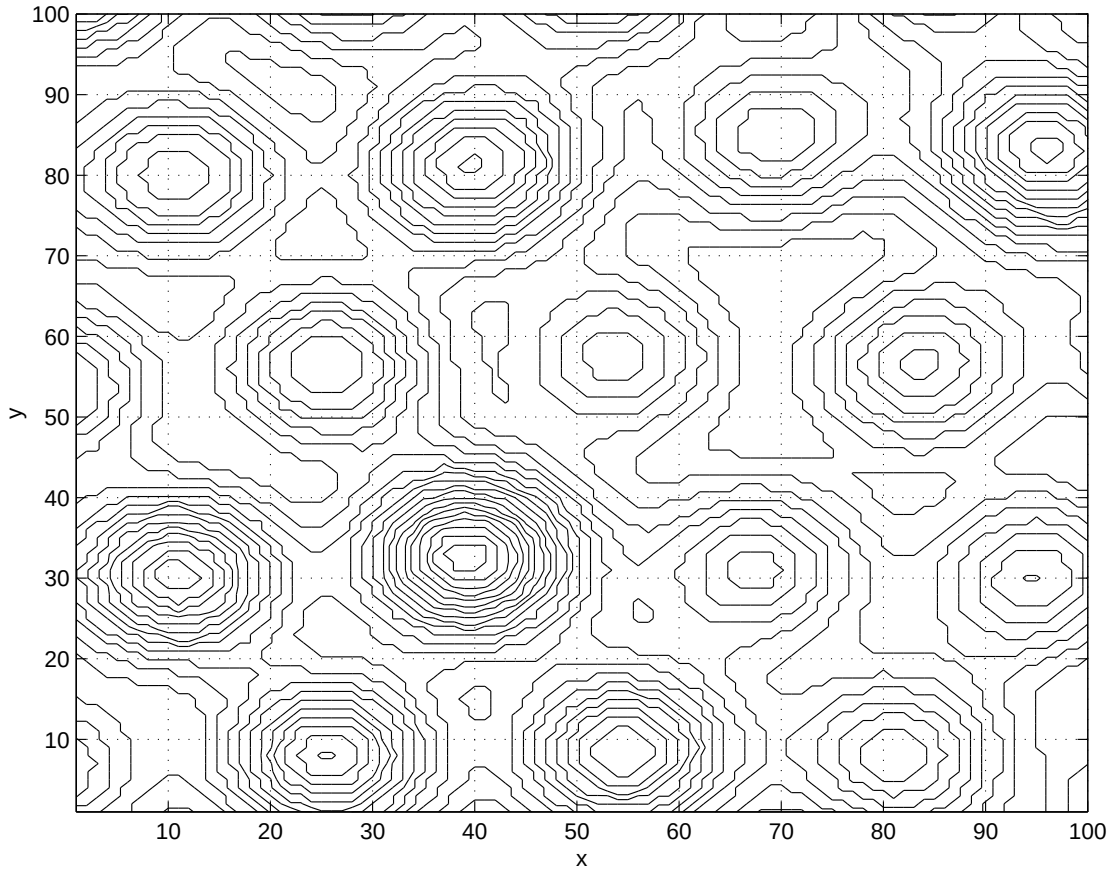
100
90
80
70
60
50
40
30
20
10
y
10
20
30
40
50
60
70
80
90
100
x

(a)

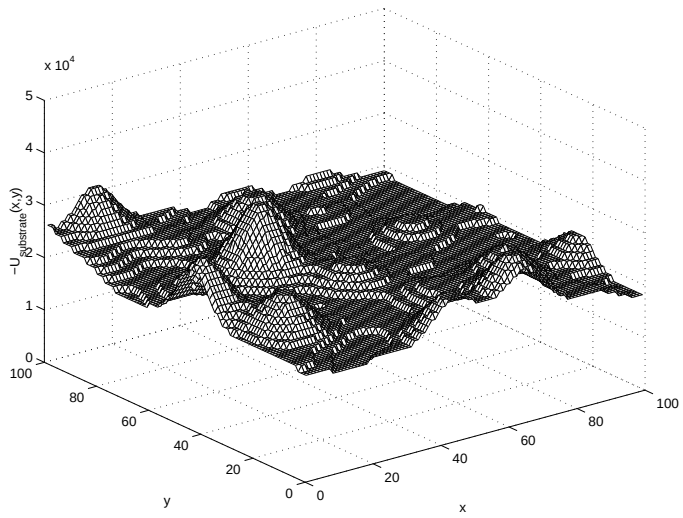
x 10^4
5
4
3
2
1
0
−U_substrate(x,y)
100
80
60
40
20
0
y
0
20
40
60
80
100
x

(b)

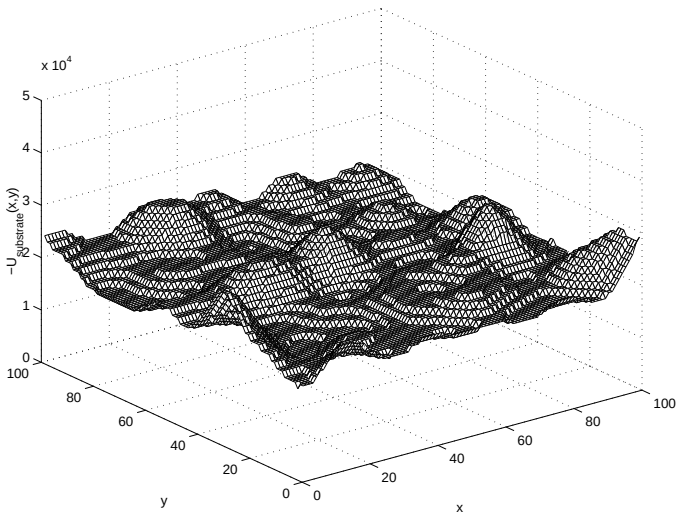
x 10^4
5
4
3
2
1
0
−U_substrate(x,y)
100
80
60
40
20
0
y
0
20
40
60
80
100
x

(c)

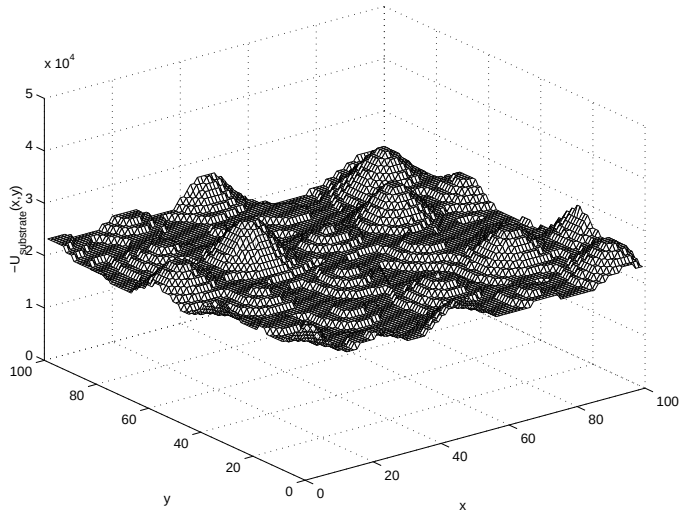
x 10^4
5
4
3
2
1
0
−U_substrate(x,y)
100
80
60
40
20
0
y
0
20
40
60
80
100
x

(d)

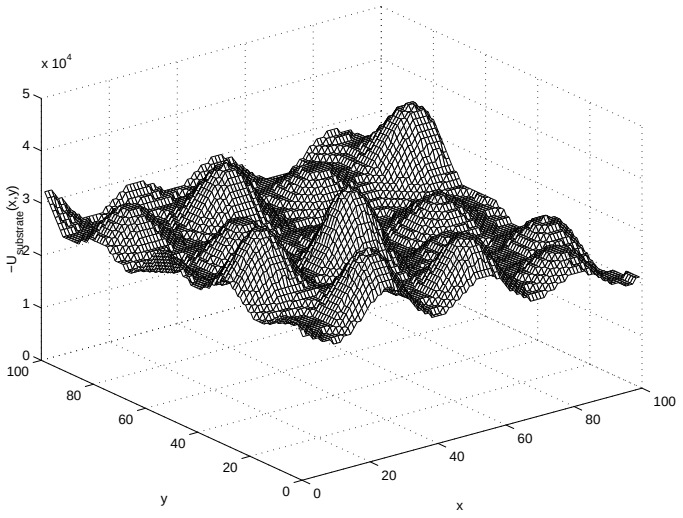
x 10^4
5
4
3
2
1
0
−U_substrate(x,y)
100
80
60
40
20
0
y
0
20
40
60
80
100
x

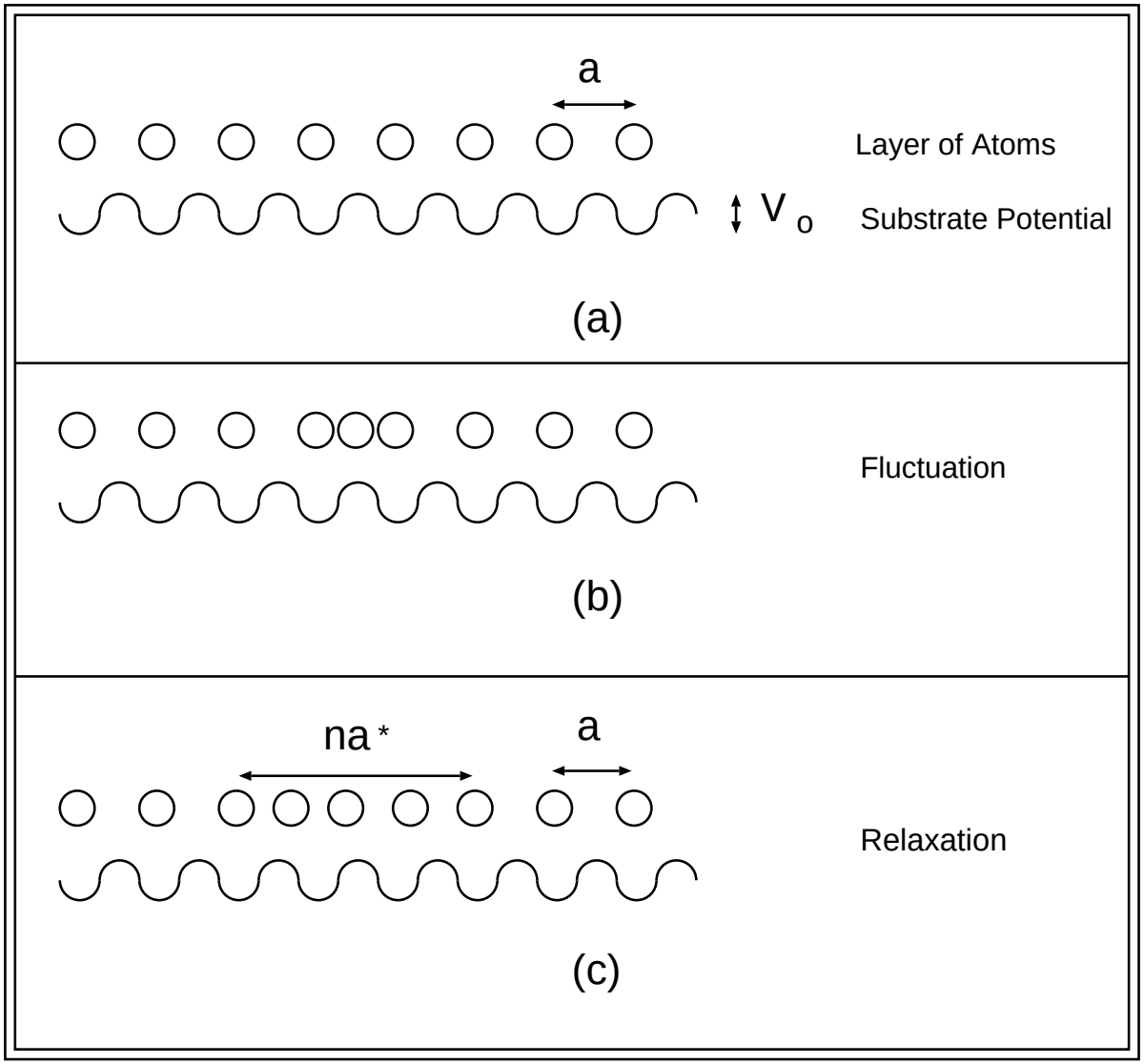
a
Layer of Atoms
V o
Substrate Potential
(a)
Fluctuation
(b)
na *
a
Relaxation
(c)

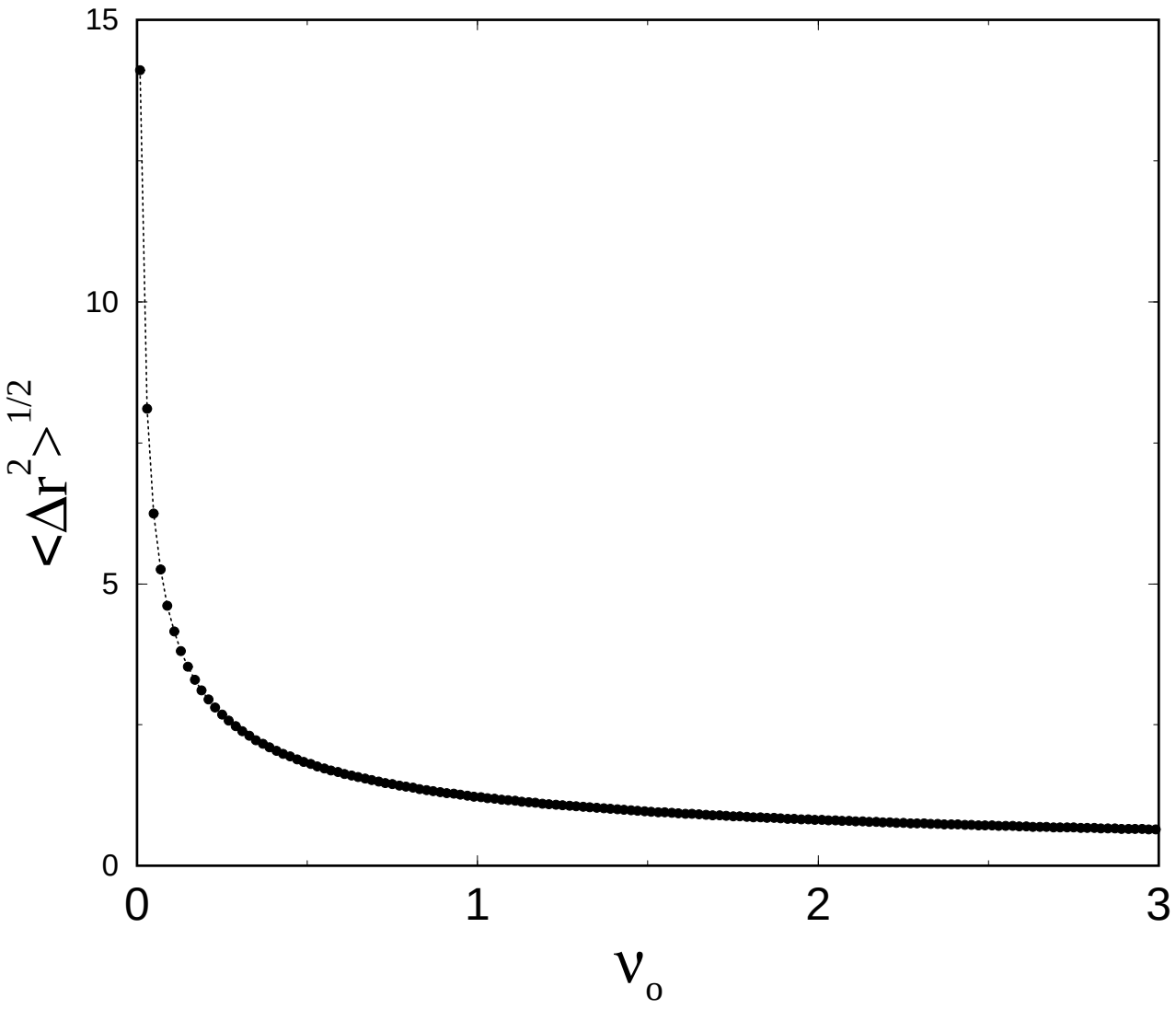
15
10
5
0
0
1
2
3
$<\Delta r^2>^{1/2}$
ν_o